



HAL
open science

Candidate type II quasars at $2 < z < 4.3$ in the Sloan Digital Sky Survey III

Rachael Alexandroff, Michael A. Strauss, Jenny E. Greene, Nadia L. Zakamska, Nicholas P. Ross, W. N. Brandt, Guilin Liu, Paul S. Smith, Jian Ge, Fred Hamann, et al.

► **To cite this version:**

Rachael Alexandroff, Michael A. Strauss, Jenny E. Greene, Nadia L. Zakamska, Nicholas P. Ross, et al.. Candidate type II quasars at $2 < z < 4.3$ in the Sloan Digital Sky Survey III. *Monthly Notices of the Royal Astronomical Society*, 2013, 435, pp.3306-3325. 10.1093/mnras/stt1500 . hal-03645447

HAL Id: hal-03645447

<https://hal.science/hal-03645447>

Submitted on 24 May 2022

HAL is a multi-disciplinary open access archive for the deposit and dissemination of scientific research documents, whether they are published or not. The documents may come from teaching and research institutions in France or abroad, or from public or private research centers.

L'archive ouverte pluridisciplinaire **HAL**, est destinée au dépôt et à la diffusion de documents scientifiques de niveau recherche, publiés ou non, émanant des établissements d'enseignement et de recherche français ou étrangers, des laboratoires publics ou privés.

Candidate type II quasars at $2 < z < 4.3$ in the Sloan Digital Sky Survey III

Rachael Alexandroff,^{1,2*} Michael A. Strauss,² Jenny E. Greene,²
Nadia L. Zakamska,¹ Nicholas P. Ross,³ W. N. Brandt,^{4,5} Guilin Liu,¹ Paul S. Smith,⁶
Jian Ge,⁷ Fred Hamann,⁷ Adam D. Myers,⁸ Patrick Petitjean,⁹ Donald P. Schneider,^{4,5}
Hassen Yesuf¹⁰ and Donald G. York¹¹

¹Center for Astrophysical Sciences, Department of Physics and Astronomy, Johns Hopkins University, Baltimore, MD 21218, USA

²Department of Astrophysical Sciences, Princeton University, Princeton, NJ 08544, USA

³Lawrence Berkeley National Laboratory, 1 Cyclotron Road, Berkeley, CA 92420, USA

⁴Department of Astronomy and Astrophysics, The Pennsylvania State University, 525 Davey Laboratory, University Park, PA 16802, USA

⁵Institute for Gravitation and the Cosmos, The Pennsylvania State University, University Park, PA 16802, USA

⁶Steward Observatory, University of Arizona, 933 North Cherry Avenue, Tucson, AZ 85721, USA

⁷Department of Astronomy, University of Florida, Gainesville, FL 32611-2055, USA

⁸Department of Physics and Astronomy, University of Wyoming, Laramie, WY 82072, USA

⁹UPMC-CNRS, UMR7095, Institut d'Astrophysique de Paris, 98bis Boulevard Arago, F-75014 Paris, France

¹⁰UCO/Lick Observatory, University of California, Santa Cruz, 1156 High Street, Santa Cruz, CA 95064, USA

¹¹Department of Astronomy and Astrophysics and the Enrico Fermi Institute, University of Chicago, 5640 South Ellis Avenue, Chicago, IL 60637, USA

Accepted 2013 August 12. Received 2013 August 9; in original form 2013 July 27

ABSTRACT

At low redshifts, dust-obscured quasars often have strong yet narrow permitted lines in the rest-frame optical and ultraviolet, excited by the central active nucleus, earning the designation type II quasars. We present a sample of 145 candidate type II quasars at redshifts between 2 and 4.3, encompassing the epoch at which quasar activity peaked in the universe. These objects, selected from the quasar sample of the Baryon Oscillation Spectroscopic Survey of the Sloan Digital Sky Survey III, are characterized by weak continuum in the rest-frame ultraviolet (typical continuum magnitude of $i \approx 22$) and strong lines of C IV and Ly α , with full width at half-maximum less than 2000 km s^{-1} . The continuum magnitudes correspond to an absolute magnitude of -23 or brighter at redshift 3, too bright to be due exclusively to the host galaxies of these objects. Roughly one third of the objects are detected in the shorter wavelength bands of the *Wide-Field Infrared Survey Explorer* survey; the spectral energy distributions of these objects appear to be intermediate between classic type I and type II quasars seen at lower redshift. Five objects are detected at rest frame $6 \mu\text{m}$ by *Spitzer*, implying bolometric luminosities of several times $10^{46} \text{ erg s}^{-1}$. We have obtained polarization measurements for two objects; they are roughly 3 per cent polarized. We suggest that these objects are luminous quasars, with modest dust extinction ($A_V \sim 0.5 \text{ mag}$), whose ultraviolet continuum also includes a substantial scattering contribution. Alternatively, the line of sight to the central engines of these objects may be obscured by optically thick material whose covering fraction is less than unity.

Key words: quasars: emission lines – quasars: general.

1 INTRODUCTION

In standard unification models, many of the observed properties of active galactic nuclei (AGN) can be explained by differences

in viewing angle (Antonucci 1993; Urry & Padovani 1995). In these models, the accretion disc of the supermassive black hole (SMBH) is surrounded by a torus of gas and dust, which, when oriented along the line of sight, obscures emission from the region around the SMBH at optical, ultraviolet and soft X-ray wavelengths. Because this gas and dust does not cover all 4π steradians around the central engine, gas in the host galaxy above and below

* E-mail: rmalexan@pha.jhu.edu

the torus is illuminated by the engine, giving rise to strong narrow high-ionization emission lines [full width at half-maximum (FWHM) $< 2000 \text{ km s}^{-1}$] and weak continua (Zakamska et al. 2003) in the rest-frame optical spectra. Such objects are classified as type II based on their optical spectra, in contrast to type I objects which show strong ultraviolet continua and broad permitted lines (Khachikyan & Weedman 1971; Khachikian & Weedman 1974). Type II AGN tend to show a high ratio of IR to optical light, to have hard X-ray spectra and to be strongly polarized, consistent with the obscuring torus hypothesis (Antonucci & Miller 1985; Norman et al. 2002; Smith et al. 2002; Zakamska et al. 2003; Brandt & Hasinger 2005). However, Sanders et al. (1988), Canalizo & Stockton (2001), Hopkins et al. (2006) and Glickman et al. (2012) argue that type I and type II quasars represent different phases in quasar evolution: in their models, all quasars pass through an obscured phase before outflows from the AGN and central star formation expel the obscuring material.

The comoving space density of luminous type I quasars peaked at redshifts 2–3 (Schmidt, Schneider & Gunn 1995; Richards et al. 2006a; Ross et al. 2013), although the demographics of luminous obscured quasars at this epoch are poorly understood. While it is straightforward to identify unobscured quasars as ultraviolet-excess sources in multiband optical surveys (Sandage 1965; Green, Schmidt & Liebert 1986; Richards et al. 2006a), a complete census of AGN is challenging at visible wavelengths alone, given that an appreciable fraction of the quasar population is obscured by dust. Astronomers have used searches in a variety of wavebands to identify obscured quasars (see, for example, Brandt & Hasinger 2005; Hatziminaoglou et al. 2005; Stern et al. 2005, 2012; Gilli, Comastri & Hasinger 2007; Treister, Urry & Virani 2009b; Vasudevan et al. 2010; Ballantyne et al. 2011; Donley et al. 2012; Xue et al. 2012; Assef et al. 2013; Mignoli et al. 2013).

The integral of the quasar luminosity function, with appropriate efficiency factors, approximately matches the present-day mass function of SMBH (Soltan 1982; Yu & Tremaine 2002; Marconi et al. 2004) indicating that black holes accrete much of their mass during a luminous phase as quasars. This argument has profound implications for understanding the growth of black holes and their role in galaxy evolution, but improving this calculation requires good measurements of quasar demographics, including the obscured quasar fraction, as a function of redshift and luminosity. This goal remains elusive: surveys at different wavelengths often find discrepant results (Lawrence & Elvis 2010). At $z < 0.8$, Reyes et al. (2008) find that the ratio of optically selected type II to type I luminous quasars is at least 1:1, while X-ray studies (for example, Ueda et al. 2003; Hasinger 2008) place the value at $\sim 3:1$ for low-luminosity active nuclei, but $< 1:1$ for high-luminosity quasars. Using X-ray data, Mushotzky et al. (2000) and Hickox & Markevitch (2006) suggest that the obscured fraction remains constant or even increases with redshift (see reviews by Ballantyne et al. 2011; Treister & Urry 2012, for further discussion).

High-redshift radio-loud type II quasars have been studied for decades (see, for example, the review paper by McCarthy 1993) but their radio-quiet counterparts in the optical, IR and X-ray have been harder to find. Deep mid-IR (e.g. Alexander et al. 2005; Stern et al. 2005, 2012; Dey et al. 2008; Coppin et al. 2010; Donley et al. 2012) and X-ray (e.g. Treister et al. 2009a; Comastri et al. 2011; Lehmer et al. 2012; Vasudevan et al. 2013) surveys tend to cover small solid angles, and are thus not sensitive to rare luminous objects. Moreover, indications of obscuration do not always agree between different wavebands (e.g., Barger et al. 2005; Civano et al. 2012; Jia et al. 2012). For example, about 50 per cent of X-ray-identified

Compton-thick objects show broad emission lines in their optical spectra (e.g. Vasudevan et al. 2009).

The Sloan Digital Sky Survey (SDSS; York et al. 2000; Eisenstein et al. 2011) has covered almost 1/3 of the celestial sphere in both visible-light imaging and spectroscopy to a depth at which significant numbers of high-redshift quasars are found (Richards et al. 2002). Zakamska et al. (2003) and Reyes et al. (2008) selected high-luminosity type II objects with $z < 0.83$ among SDSS spectra of galaxies (Strauss et al. 2002) and Faint Images of the Radio Sky at Twenty-cm (FIRST) radio sources (Becker, White & Helfand 1995). These objects were identified by their strong narrow emission lines (FWHM less than 1000 km s^{-1} in most cases) and weak continuum; $[\text{O III}]5008 \text{ \AA}$ was used as a crude proxy for bolometric luminosity (Heckman et al. 2005). Additional observations of these objects, including spectropolarimetry (Zakamska et al. 2005, 2006) and mid-infrared photometry and spectroscopy (Zakamska et al. 2008) demonstrated that these objects were indeed highly luminous obscured quasars, with a space density (at least to $z \sim 0.8$) comparable to unobscured quasars (Reyes et al. 2008).

Searches for counterparts at higher redshift were not successful in the SDSS-I/II data; narrow-line objects typically had strong continua and extensive Fe emission, showing them to be high-redshift analogues of Narrow-Line Seyfert I galaxies (NLS1; Osterbrock & Pogge 1985; Williams, Pogge & Mathur 2002). However, the Baryon Oscillation Spectroscopic Survey (BOSS; Dawson et al. 2013) of SDSS-III (Eisenstein et al. 2011) targets quasars two magnitudes fainter than SDSS-I/II did (Ross et al. 2012), probing to continuum levels at which type II quasar candidates at high redshift begin to appear.

In this paper, we describe a class of high-redshift ($z > 2$) type II quasar candidates identified by their characteristic spectra from BOSS. We have found 452 candidates with redshifts in the range $2.03 < z < 4.23$ in the SDSS-III Data Release 9 (hereafter referred to as DR9; Ahn et al. 2012). We describe the relevant SDSS data in Section 2 and the selection of our candidates in Section 3. The properties of these objects in SDSS data are described in Section 4, and we match against other data sets in Section 5. We discuss our results in Section 6 and conclude in Section 7. We assume a flat Λ CDM cosmology with $\Omega_m = 0.26$, $\Omega_\Lambda = 0.74$ and $h = 0.71$ (Spergel et al. 2007) throughout this paper. We use AB magnitudes consistently in this paper.

2 SDSS OBSERVATIONS AND DATA PROCESSING

The SDSS has been in routine operation since 2000. It uses the dedicated 2.5-metre wide-field Sloan Foundation Telescope at Apache Point Observatory in New Mexico (Gunn et al. 2006), carrying out both imaging (Gunn et al. 1998) and spectroscopy. The two optical spectrographs were upgraded in 2009 for the BOSS survey (Smee et al. 2013); each is fed by 500 optical fibres with 2 inch optical diameter, yielding spectrophotometrically calibrated spectra from 3600 to $10\,400 \text{ \AA}$,¹ with resolution $\lambda/\Delta\lambda \approx 1800$. BOSS is designed to measure the baryon oscillation feature in the clustering of

¹ As described in Pâris et al. (2012) and Dawson et al. (2013), fibres for quasar candidates in BOSS were often offset from their fiducial positions to maximize the throughput in the blue given differential chromatic refraction. However, the spectrophotometric standard stars were observed without these offsets, causing systematic errors in the spectrophotometric calibration of quasars of up to 40 per cent.

galaxies (Anderson et al. 2012) and the Ly α absorption spectra of quasars (Busca et al. 2013).

BOSS data were first made public in the SDSS DR9, containing spectra of 536 000 galaxies and 102 000 quasars over 3275 deg². Because of the need to observe the Ly α forest, quasars are targeted in the region of colour space where objects with $2.15 < z < 3.5$ are expected to lie (Ross et al. 2012). This is a challenging task, because the broad-band colours of $z \sim 2.7$ quasars are similar to those of much more numerous F and A stars (Fan 1999). The quasar candidates are selected to a point source function magnitude limit of $g \leq 22.0$ or $r \leq 21.85$ (after correction for extinction in Schlegel, Finkbeiner & Davis 1998). All spectra are processed with a common pipeline (Bolton et al. 2012); Pâris et al. (2012) report that almost 97 per cent of quasar targets have spectra of sufficient signal-to-noise ratio (S/N) to measure a reliable redshift.

At redshifts above $z \sim 1$, the H α , H β and [O III] emission lines commonly used as diagnostics for identifying type II quasars at optical wavelengths no longer fall within the wavelength coverage of the BOSS spectrograph. Instead, we used the widths of the Ly α (1216 Å) and C IV (1549 Å) emission lines as diagnostics of candidate type II objects, making a cut at $\text{FWHM} < 2000 \text{ km s}^{-1}$ (see, e.g., Zakamska et al. 2003; Hao et al. 2005; Sulentic et al. 2007). Given the BOSS spectral coverage, we can measure Ly α cleanly at redshifts $z \gtrsim 2.0$. Line widths are measured directly by the BOSS pipeline, from single Gaussian fits to the Ly α and C IV lines.

3 SAMPLE SELECTION CRITERIA

Heavily dust-obscured quasars are expected to have strong, narrow emission lines atop a relatively weak continuum, which is a combination of the light from the host galaxy and the light from the hidden quasar scattered by the interstellar material in the host. The classical definition of optically selected type II active nuclei largely focuses on the widths and ratios of emission lines, which is the approach that Reyes et al. (2008) used in selecting ~ 900 type II quasars at $z < 0.8$ from SDSS-I/II data. But because obscured quasars are faint at rest-frame optical and ultraviolet wavelengths, previous searches for type II quasars at higher redshifts using the SDSS-I/II data have been largely unsuccessful. The redshift range between 0.8 and 2.0 is particularly difficult because none of the strong emission lines characteristic of type II quasars appear at the optical wavelengths. Only one candidate, SDSS J085600.88+371345.5 at $z = 1.02$ was identified in the original SDSS quasar sample as satisfying all our emission-line criteria. This object was also identified as an obscured quasar candidate by Gilli et al. (2010). At redshifts > 2.0 , a search for narrow-line objects in the SDSS-I/II quasar sample (Schneider et al. 2010) yielded a number of NLS1, but little else.

The BOSS survey goes substantially deeper than SDSS-I/II in spectroscopy, allowing us to resume the search for type II quasars at high redshifts based on rest-frame ultraviolet spectra. In this paper, we adopt a composite approach based both on the properties of emission lines and on the properties of the continuum. For our parent sample, we selected all BOSS objects in DR9 with both Ly α and C IV emission-line measurements (given the BOSS wavelength coverage, this corresponds to redshifts of $z \gtrsim 2.0$) and a reliable pipeline fit (i.e. the flag ZWARNING = 0; see the discussion in Bolton et al. 2012). A total of 79 505 objects satisfied these criteria. Objects with $\text{FWHM} < 2000 \text{ km s}^{-1}$ are quite rare, representing only 3.7 per cent of the total in the BOSS sample. These numbers are summarized in Table 1.

From this sample, we selected only those objects with 5σ detections in both Ly α and C IV (thus we are insensitive to objects

Table 1. Selection of type II candidates.

Sample	No. of objects
All BOSS DR9 quasars	102 100
BOSS DR9 quasars with Ly α , C IV measured	79 505
$\text{FWHM}_{\text{C IV}} < 2000 \text{ km s}^{-1}$	2494
Class A	145
Class B	307

that emit only in Ly α ; see, for example, Hall et al. 2004), and restricted ourselves to those objects in which both lines have $\text{FWHM} < 2000 \text{ km s}^{-1}$. The widths of the two lines are correlated, although the correlation is weak, due in part to absorption features (Section 4.4) and limited S/N. We then visually inspected the spectra of the 2494 remaining candidates. The best type II quasar candidates have narrow but strong emission lines and an extremely weak, flat continuum (see Fig. 1). There were two main astrophysical contaminants in our original sample: high-redshift analogues to NLS1 galaxies, and broad absorption line (BAL) quasars whose emission lines are mostly absorbed away, leaving only a narrow component in emission (Fig. 2). The rest-frame ultraviolet spectra of NLS1s (Constantin & Shields 2003) show narrow permitted lines, but possess a strong blue continuum and emission from Fe II complexes that are not seen in obscured quasars; see for example the upper panel of Fig. 2. An example of a BAL quasar whose emission line widths met our initial criteria is found in the middle panel of Fig. 2; the C IV line is clearly truncated by the associated absorption.

We classified our type II quasar candidates, after removing the BAL quasars and obvious NLS1, in two categories: those that showed all the qualities of an obscured quasar (narrow emission lines, no associated absorption, weak continuum), hereafter class A; and those with one or more characteristics of unobscured objects (a broad component to an emission line, an absorption feature or a strong blue continuum), hereafter class B. Fig. 1 presents an example of an object from class A, while the lower panel of Fig. 2 shows the spectrum of a class B object. The class B object has very narrow emission lines and weak continuum, but strong narrow absorption blueward of C IV. These classifications are S/N dependent and are somewhat subjective, and there are no doubt objects we have placed in each category that belong in the other (see Fig. 3 and the discussion in Section 4.2).

Are our type II candidate objects truly obscured quasars, in the sense of having bolometric luminosities much larger than inferred from the optical data? Our objects have line widths up to 2000 km s^{-1} , while low-redshift Seyfert II galaxies typically have line widths less than 1200 km s^{-1} (Hao et al. 2005). However, outflows in the narrow-line region may give significantly larger widths in more luminous objects, with spatial extents as large as 10 kpc (e.g. Greene, Zakamska & Smith 2012; Liu et al. 2013). We will see in what follows that the obscured nature of our objects remains unclear, and it is possible that our sample is somewhat heterogeneous, with more than one population contributing. With all this in mind, we consistently refer to our objects as type II candidates.

Fig. 3 shows the correlation between the rest-frame equivalent width and FWHM of the C IV line for each sample. The distribution of objects identified as type II quasar candidates peaks at much smaller values of C IV FWHM than either contaminating sample, but there is significant overlap among the three distributions. An initial cut at a smaller C IV FWHM would have increased our fraction of

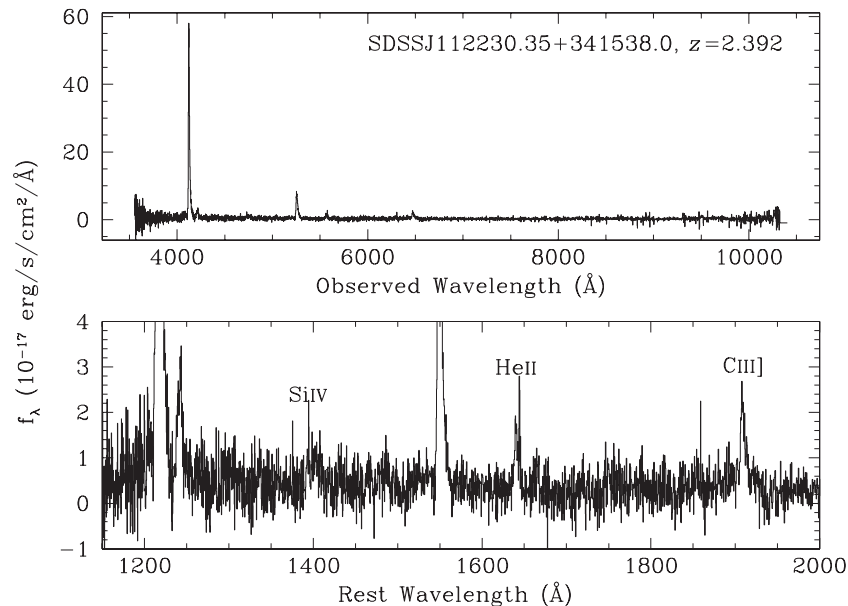


Figure 1. BOSS spectrum of a type II quasar candidate at $z \sim 2.4$; this is a typical object in class A. Note the strong narrow emission lines (Ly α and C IV have FWHM of 1000 and 1200 km s $^{-1}$, respectively) and weak continuum. The upper panel shows the full spectrum in observed wavelengths, while the lower panel expands the horizontal and vertical scales and plots rest-frame wavelengths, with emission lines identified. In this and subsequent figures, the spectra have not been smoothed.

identified type II quasar candidates but would have also excluded many strong candidates.

The Bolton et al. (2012) pipeline redshifts are determined by fits to a linear combination of templates that do not include narrow-line quasars. The asymmetries seen in Ly α due to the onset of the Ly α forest, and especially in C IV due to winds (Richards et al. 2011) in broad-line objects are not present for the objects in our sample, meaning that the redshifts based on these templates are often biased high by the order of 0.005. The DR9 quasar catalogue (Pâris et al. 2012) includes redshifts measured directly from a Gaussian fit to the C IV line, which usually lines up well with the redshift measured from Ly α and fainter lines such as C III] in our narrow-line objects. We thus use the C IV redshift when available in the DR9 quasar catalogue, and a redshift based on visual inspection in the rare cases where it is not.

4 PROPERTIES OF TYPE II QUASAR CANDIDATES: SDSS DATA

Fig. 4 shows spectra of further examples of objects in our class A sample, including one of the highest redshift objects in the sample, and the objects with the strongest and narrowest emission lines.

Our sample includes 452 objects that are strong or possible type II quasars. We list the 145 class A candidates in Table 2 and the 307 class B candidates in Table 3. Coordinates are given in J2000. The median FWHM of the C IV line among the class A candidates is 1260 km s $^{-1}$. The line parameters are as measured by the BOSS pipeline (Bolton et al. 2012); null values correspond to problems with the measurement. The mean redshift of these two samples is 2.70, with a redshift range from 2.03 to 4.23 (see Fig. 5). In what follows, we concentrate on the class A sample.

Fig. 5 shows the continuum ($\lambda = 1450$ Å) luminosity density distribution for our candidates, as well as for those objects we identified as NLS1s and BALs. These continuum luminosities, which are measured from the BOSS spectra, are significantly larger than would

be expected from the host galaxy of the quasars; the most luminous non-active galaxies at these redshifts have absolute ultraviolet continuum magnitudes of -22.5 (Shapley 2011). For comparison, the type I quasar luminosity function has been measured down to $M = -25$ at these redshifts from the BOSS survey (Ross et al. 2013). The high luminosities of our objects, together with the quasar-like broad-band colours (see discussion in Section 4.1 and Fig. 6), suggest that the quasar continuum of these objects is not completely extinguished. These objects may have only a modest dust column, or perhaps the observed continuum is due to light from the central engine that is reflected into our line of sight by dust in the quasar host galaxy, as is found in lower redshift type II quasars (Zakamska et al. 2006). A third possibility is that the extinction is patchy, with unextinguished light showing through holes in the obscuring dust.

4.1 Broad-band colours

Almost all the objects in both class A and class B were selected for spectroscopy as quasar candidates, using the algorithms described in Ross et al. (2012). There are four principal algorithms used, but 60 per cent of the objects in our sample were selected using the likelihood algorithm of Kirkpatrick et al. (2011) and the probabilistic algorithm of Bovy et al. (2011), both of which use the distribution of objects in colour space, incorporating information on photometric errors. The broad-band colours of ordinary quasars as a function of redshift are a reflection of the blue continuum, absorption by the Ly α forest and Lyman-limit systems, and, to a lesser extent, emission lines in the various bands (Fan 1999; Richards et al. 2003). Understanding the demographics of obscured quasars will require quantifying the biases that the target selection algorithms impose on the sample.

SDSS imaging is carried out in five bands, *ugriz* (Fukugita et al. 1996). Fig. 6 shows the dependence of colour on redshift, both for our sample of type II quasars, and the full sample of DR9

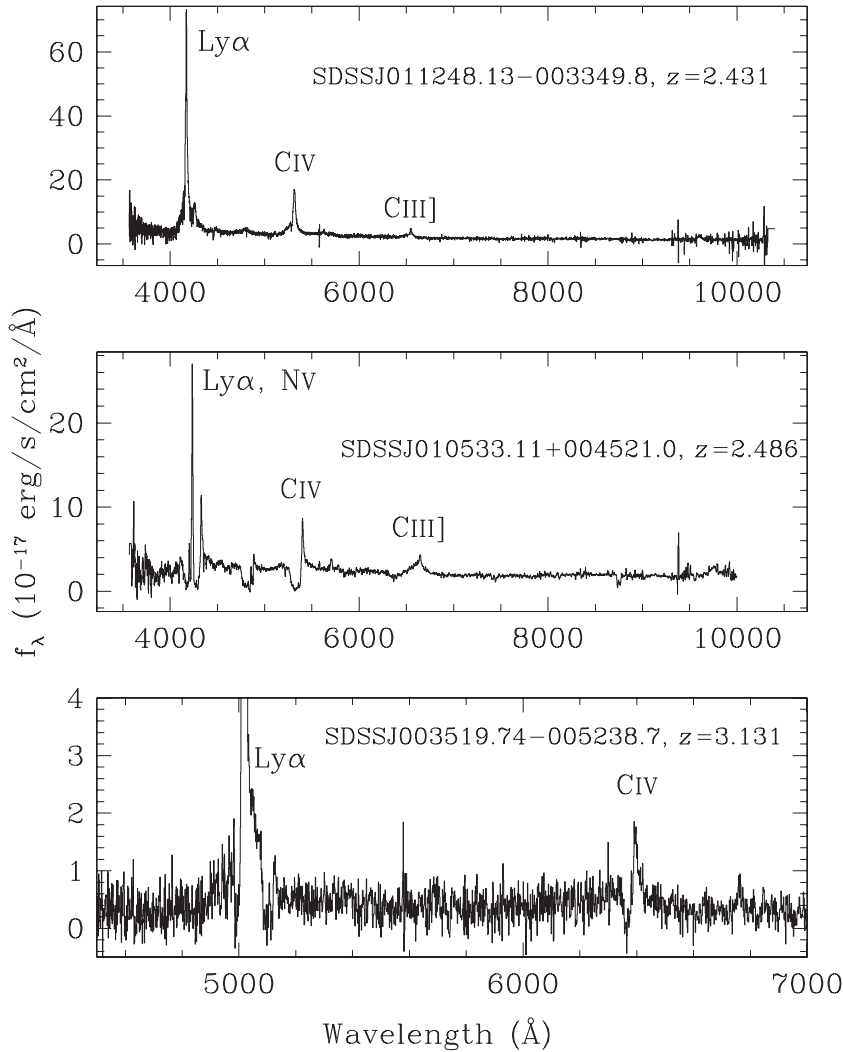


Figure 2. Upper: a narrow-line BOSS object that we classified as an NLS1; note the strong blue continuum. The C IV and Ly α lines have FWHM of 1680 and 1960 km s⁻¹, respectively, as measured by the SDSS pipeline. Middle: spectrum of a BAL quasar identified in our sample of candidates. The C IV emission line is truncated by the extensive blueward absorption; similar absorption troughs are seen in Si IV, N v and (to a lesser extent) in C III]. The C IV emission line has a FWHM from the Gaussian fit of 900 km s⁻¹; Ly α is significantly broader, at 1900 km s⁻¹. Lower: an object from our class B sample; note the expanded axes. C IV is strongly truncated by narrow absorption.

quasars (Pâris et al. 2012). The mean colours of the two groups are roughly the same, suggesting that the continua of objects in our sample are quasar like. Of course, these objects were selected by their broad-band colours, and it perhaps not surprising that their colours are similar to those of other objects selected in the same way. The rest-frame equivalent widths of Ly α , typically the strongest line in these objects, can be as large as 1000 Å, at which point the line starts significantly affecting the broad-band colours.

As the Ly α break enters the g band at $z \sim 3.5$, the $g - r$ colours quickly redden with redshift. To quantify the similarity of the colours to unobscured quasars, we selected a subsample of DR9 quasars with similar i -band magnitude distribution as our type II quasar candidates, so that they have similar photometric errors. Only objects from our sample and the DR9 catalogue with a redshift of $z \leq 3.5$ were used in the comparison, so the colour was close to constant over the whole sample. A Kolmogorov–Smirnov (K-S) test of the $g - r$ colour for each sample shows that the two distributions are the same at the 84 per cent confidence level; thus,

the colours of our objects are consistent with having been drawn from the distribution of unobscured quasars.

4.2 Composite spectrum

The upper and middle panels of Fig. 7 show the arithmetic average spectrum of our 145 class A type II quasar candidates. This average is calculated by shifting all spectra to the rest frame, and inverse-variance weighting the spectra at a given wavelength, using errors estimated by the SDSS spectroscopic pipeline.

We used the program MPFIT (Markwardt 2009) in IDL to fit one or two Gaussian components and a local continuum around each emission line in the composite spectra. C IV was fitted with two Gaussians corresponding to a broad- and narrow-line component, after masking any associated absorption blueward of the emission line. Other than Ly α , the redshifts and widths of emission lines were constrained to be the same as that of C IV. The Ly α N v, He II and C III] lines were also each fitted with two Gaussian components, while all other emission lines were fitted with only a single Gaussian

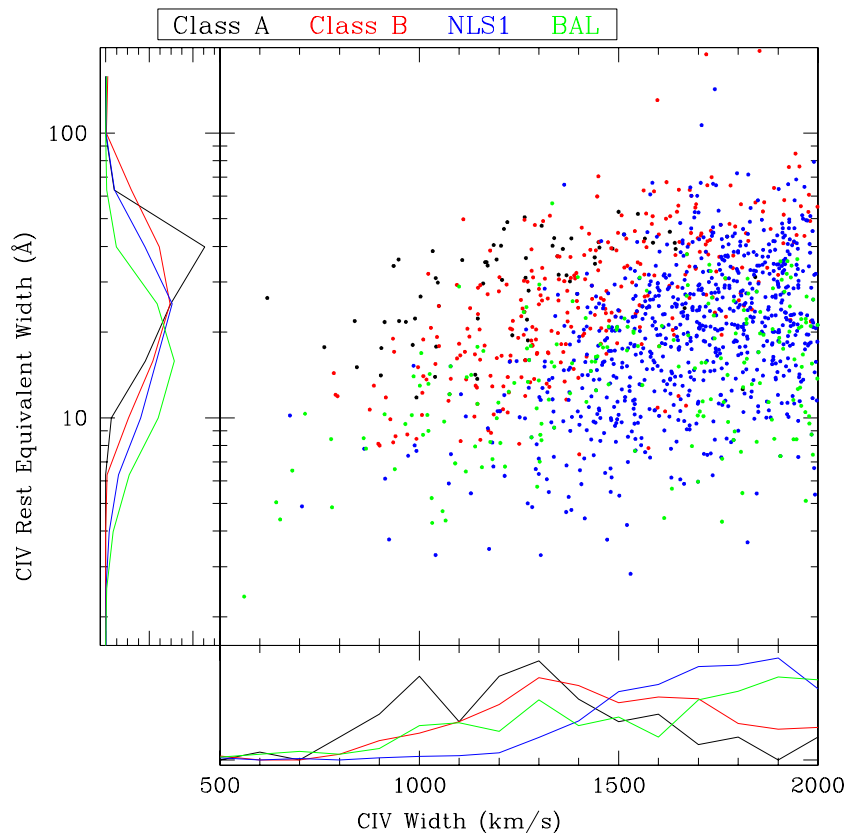


Figure 3. The FWHM and rest-frame equivalent width (EW) of the $C_{IV} \lambda 1549 \text{ \AA}$ line for all 2494 objects in DR9 with $\text{FWHM} < 2000 \text{ km s}^{-1}$ and 5σ detection of both $\text{Ly}\alpha$ and C_{IV} emission lines. Type II quasar candidates are shown with class A objects in black and class B objects in red (see the discussion in Section 4), NLS1s are shown in blue and BALs in green. The distributions of each quantity (normalized to the same integral) are plotted on the sides. The class A and class B objects tend to have considerably lower FWHM and higher equivalent width than the NLS1 and the BALs.

component. $\text{Ly}\alpha$ was fitted simultaneously with N_{IV} , Si_{IV} simultaneously with O_{IV} and C_{III} simultaneously with both Si_{III} and Al_{III} . The resulting fluxes are listed in Table 4, and the measured emission line widths are listed in Table 5. The continuum level in the composite is constant at about $0.4 \times 10^{-17} \text{ erg s}^{-1} \text{ cm}^{-2} \text{ \AA}^{-1}$, so rest-frame equivalent widths in Angstroms are roughly the listed flux value, times 2.5.

Interestingly, the $\text{Ly}\alpha$ and C_{III} emission lines in our composite type II candidate spectrum show a broad base ($\text{FWHM} > 3000 \text{ km s}^{-1}$; Table 5), as does C_{IV} after masking absorption blueward of the line. The flux in this broad component is comparable to the narrow component, as Table 4 makes clear. This absorption and broad base were among the qualities that caused us to classify some of our candidates as class B; at higher S/N, it is likely that many of the individual class A objects would show broad components or associated C_{IV} absorption. The composite spectrum of our NLS1s shows significantly stronger broad bases on all of the emission lines as well as a significantly higher continuum flux relative to the emission lines. In addition, absorption blueward of C_{IV} is particularly strong.

The middle panel of Fig. 7 expands the vertical and horizontal scales to make weaker emission lines visible. We detect features that are usually blended in quasar spectra (Vanden Berk et al. 2001; see also the discussion in Hewett & Wild 2010), such as the $\text{Si}_{IV} \lambda\lambda 1393, 1402 \text{ \AA}$ doublet and $C_{III} \lambda 1909 \text{ \AA}$, $\text{Si}_{III} \lambda 1892 \text{ \AA}$ and $\text{Al}_{III} \lambda 1857 \text{ \AA}$, are resolved. The $N_{IV} \lambda 1486 \text{ \AA}$ line, which is only rarely seen in type I AGN (Bentz, Hall & Osmer 2004; Jiang, Fan &

Vestergaard 2008), but is seen in high-redshift radio galaxies (Humphrey et al. 2008) and low-luminosity type II AGN (Hainline et al. 2011) is present. There is little evidence for the Fe_{II} emission complexes blueward of Mg_{II} (Vanden Berk et al. 2001). The mean type II candidate spectrum is blue in f_{λ} , although not as blue as in NLS1s. The continuum break due to the $\text{Ly}\alpha$ forest is clearly visible.

There are weak absorption features apparent in this composite, but they mostly appear blueward of emission lines, representing outflows from the central engine or the superposition of individual absorption features (Nestor, Hamann & Rodriguez Hidalgo 2008), rather than stellar or interstellar medium lines. At high S/N, the spectra of Lyman-break galaxies (LBGs) also show absorption lines in the rest-frame ultraviolet, as is apparent in the composite spectrum of Shapley et al. (2003); high-ionization absorption lines have also been seen in high-redshift type II AGN (Steidel et al. 2002; Hainline et al. 2011). In LBGs, resonance absorption in the interstellar medium tends to be blueshifted by several hundred km s^{-1} , indicating strong outflows presumably powered by starbursts. In our composite, the only absorption feature that appears to coincide with those in LBGs is $\text{Si}_{IV} \lambda 1396 \text{ \AA}$, as shown in the lowest panel of Fig. 7; the absorption is considerably blueward of the emission line, corresponding to a blueshift of order 2000 km s^{-1} (the absorption feature blueward of C_{IV} is also offset by $\sim 2000 \text{ km s}^{-1}$). Moreover, it is unclear what is the driving source of these outflows (processes in the host galaxy or the central engine) and whether they are occurring on the galactic or on the circumnuclear scale.

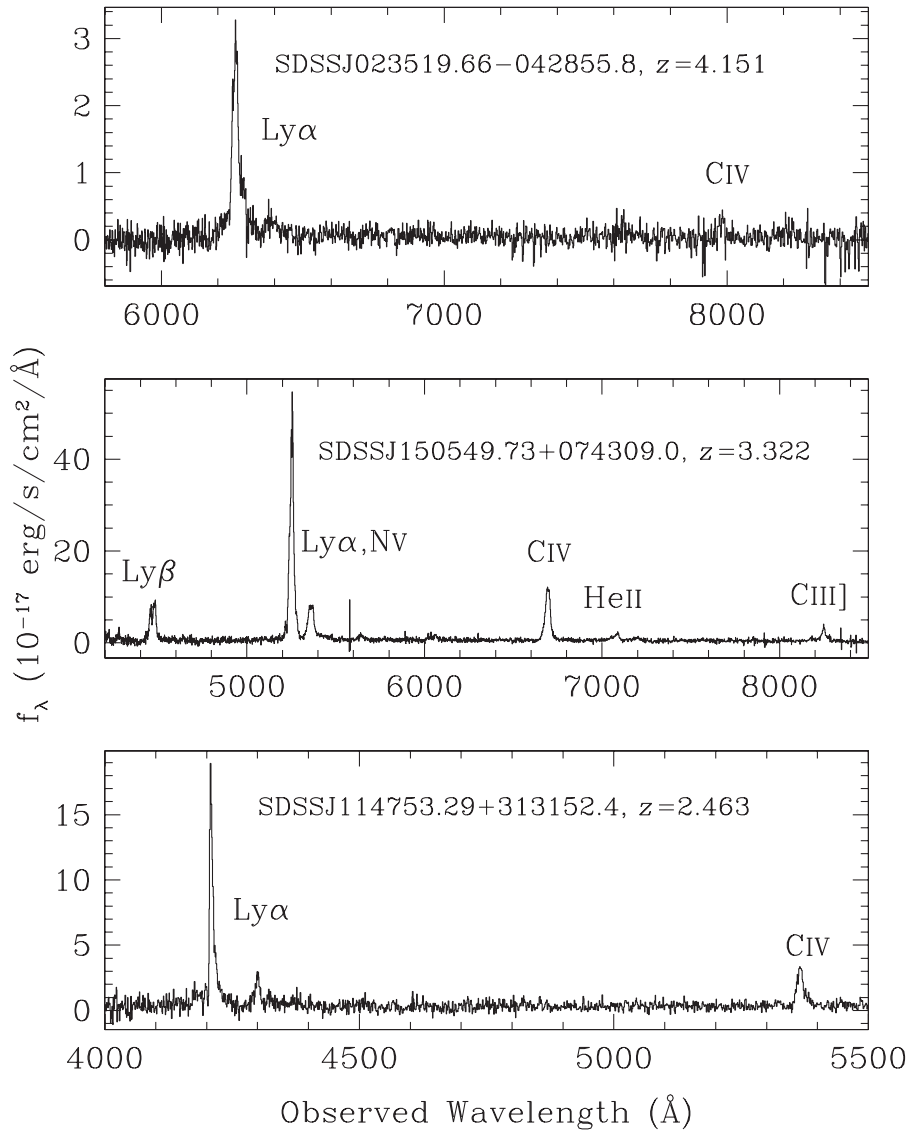


Figure 4. The BOSS spectra of some of the notable objects in the class A sample of type II quasar candidates. Top: one of the highest-redshift objects in our sample. C IV is barely detected. Middle: one of the objects with highest emission-line flux. Bottom: this object has among the narrowest emission lines in the sample (540 km s^{-1} in Ly α and 950 km s^{-1} in C IV). It also has the reddest continuum in the sample.

Table 2. Table of 145 class A candidate type II quasars.

SDSS J2000 name	RA (°)	Dec. (°)	Redshift	C IV FWHM (km s^{-1})	C IV REW (Å)	C IV flux ($10^{-17} \text{ erg s}^{-1} \text{ cm}^{-2}$)	Ly α flux ($10^{-17} \text{ erg s}^{-1} \text{ cm}^{-2}$)
SDSS J001040.82+004550.5	2.670 08	0.7640	2.7148	1507 ± 59	43.9 ± 0.0	73.3 ± 2.8	248 ± 2.9
SDSS J001738.55-011838.7	4.410 64	-1.3108	3.2260	768 ± 52	25.2 ± 0.5	21.3 ± 1.4	101.3 ± 2.3
SDSS J001814.72+023258.8	4.561 34	2.5497	2.9024	874 ± 97	19.1 ± 0.8	16.67 ± 1.9	143.6 ± 3.0
SDSS J003605.26+001618.7	9.021 93	0.2719	2.9503	1773 ± 294	12.3 ± 1.5	18.7 ± 3.0	76.2 ± 2.4
SDSS J004423.20+035715.5	11.096 65	3.9543	2.2213	1182 ± 47	Null	74.3 ± 3.0	416.8 ± 7.8
SDSS J004600.48+000543.6	11.501 99	0.0955	2.4560	1286 ± 61	28.1 ± 0.5	50.3 ± 2.5	225.2 ± 3.9

Only a portion of this table is shown here to demonstrate its form and content. A machine-readable version of the full table will be published online as Supporting Information.

4.3 Comparison to other samples of obscured quasars

We now compare the spectral properties of our objects to those of other obscured AGN samples in the literature. Hainline et al. (2011) have identified 33 AGN selected by their ultraviolet emission-line properties from a spectroscopic survey of star-forming galaxies at

$z \sim 2-3$. These objects, all of which show narrow emission lines, are significantly fainter than ours, with typical continuum brightnesses of $R \sim 24$. The ultraviolet/optical spectral energy distributions (SEDs) of these galaxies are well fitted by stellar population synthesis models with no AGN component (Hainline et al. 2012).

Table 3. Table of 307 class B candidate type II quasars.

SDSS J2000 name	RA ($^{\circ}$)	Dec. ($^{\circ}$)	Redshift	C IV FWHM (km s^{-1})	C IV REW (\AA)	C IV flux ($10^{-17} \text{ erg s}^{-1} \text{ cm}^{-2}$)	Ly α flux ($10^{-17} \text{ erg s}^{-1} \text{ cm}^{-2}$)
SDSS J001008.02+000317.5	2.533 41	0.054 85	2.2918	1655 ± 21	Null	219.4 ± 2.8	477.0 ± 4.7
SDSS J001142.42-000845.7	2.926 75	-0.146 02	2.3146	1154 ± 64	11.3 ± 0.4	39.0 ± 2.0	135.5 ± 3.3
SDSS J001344.04+011456.0	3.433 49	1.248 89	2.2250	1590 ± 42	Null	95.9 ± 2.4	237.2 ± 4.4
SDSS J001922.82-004938.2	4.845 07	-0.827 27	3.3060	968 ± 68	8.7 ± 0.4	28.6 ± 2.0	218.3 ± 3.1
SDSS J003519.74-005238.7	8.832 24	-0.877 42	3.1290	1086 ± 85	Null	25.5 ± 1.9	166.7 ± 2.5
SDSS J003809.47+031634.1	9.539 44	3.276 15	2.4644	1173 ± 118	8.8 ± 0.7	34.0 ± 3.5	187.9 ± 5.2
SDSS J005018.67+050132.5	12.5778	5.025 71	2.9370	1149 ± 75	12.8 ± 0.6	46.0 ± 3.2	214.7 ± 3.2

Only a portion of this table is shown here to demonstrate its form and content. A machine-readable version of the full table will be published online as Supporting Information.

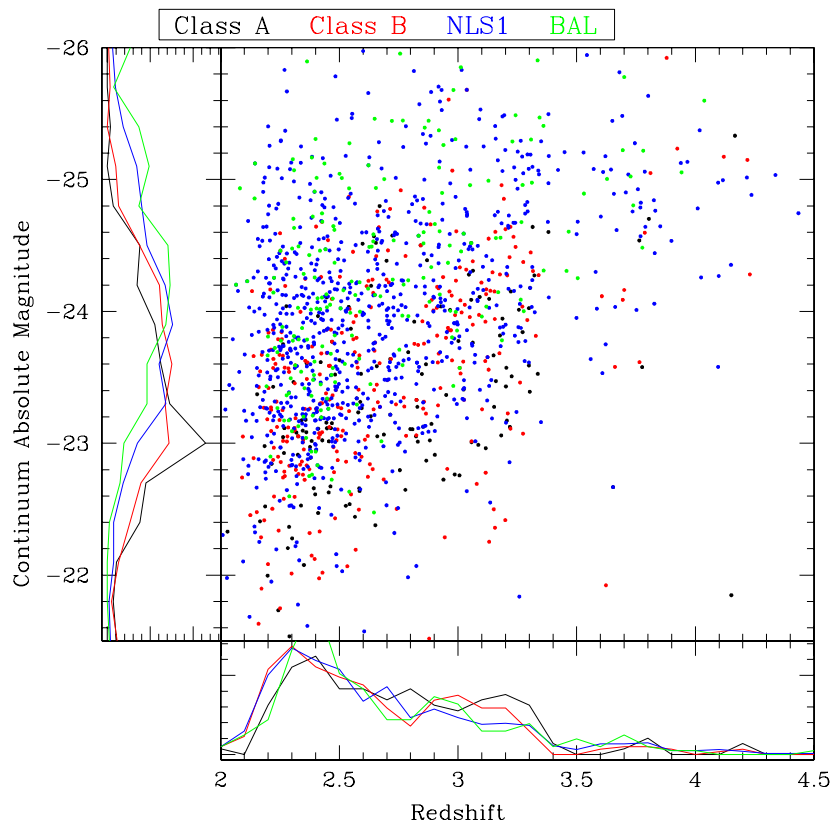


Figure 5. Two-dimensional distribution of redshift and continuum absolute magnitude (calculated at a rest wavelength of $\lambda = 1450 \text{ \AA}$) for all type II quasar candidates in our sample. The colour-coding is the same as in Fig. 3. Normalized distributions of each individual quantity are shown on the side. The continuum luminosities are measured from the spectra; uncertainties in the spectrophotometric calibration are as large as 40 per cent. The type II quasar candidate continuum absolute magnitude distribution indicates that both the class A objects and the class B objects tend to be fainter than the other two samples, as we would expect for obscured objects. The redshift distributions of the samples are similar to one another, and to the parent DR9 quasar sample overall.

Their composite spectrum is shown in the middle panel of Fig. 7, arbitrarily normalized to have a similar continuum at 1700 \AA as our composite, allowing an approximate comparison of the rest-frame equivalent widths of emission lines in the two composites. The emission lines in the Hainline et al. composite show no evidence for a broad base in Ly α or C IV. Unlike our type II candidates, there is no hint of contamination from an unobscured component. However, objects from the Hainline et al. sample have emission line widths comparable to the narrow component of the class A composite. One is also struck by the significantly greater strength of all emission lines in the class A composite; Ly α (which goes off-scale in this expanded view) peaks at $\sim 7 \times 10^{-17} \text{ erg s}^{-1} \text{ cm}^{-2} \text{ \AA}^{-1}$ in the normalized Hainline et al. composite, and $14 \times 10^{-17} \text{ erg s}^{-1} \text{ cm}^{-2} \text{ \AA}^{-1}$

in the class A objects. The one exception is the He II line at 1640 \AA , which is comparable in strength in the two composites; we will discuss this line further below.

The peaks of Ly α , C IV and most weaker lines of our composite align well with those of the type II composite from Hainline et al., with the interesting exception of the Si IV $\lambda\lambda 1394, 1403 \text{ \AA}$ doublet (lower panel of Fig. 7) which is redshifted in the Hainline et al. composite relative to ours by 800 km s^{-1} . A similar redshift is present in the [O I]/[Si II] 1302 \AA blend as well. Excess absorption due to outflows in Hainline et al. objects would suppress the blue wings of the emission features and shift them systematically to the red, although the amount of shift seems extreme. Moreover, the composite of our class A objects also shows absorption, but nevertheless the emission

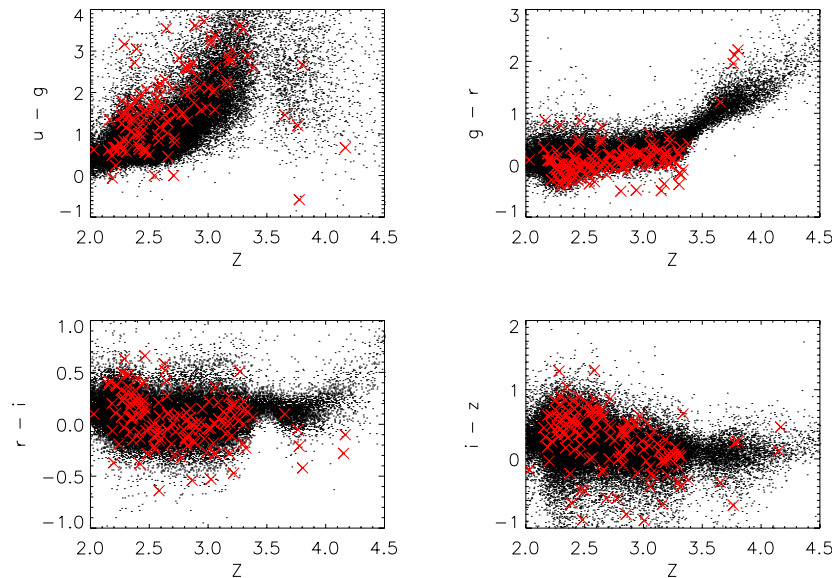


Figure 6. SDSS colours as a function of redshift for all BOSS quasars in DR9 (black dots), and the 145 class A type II quasar candidates (red crosses). A K-S comparison of the $g - r$ colour distribution of the $z < 3.5$ sample with a subsample of type I quasars matched in the i -band magnitude shows that both populations are drawn from the same distribution with 84 per cent confidence. This result suggests that the continuum is more quasar-like than galaxy-like.

peaks at exactly the expected wavelengths. Indeed, the Si IV lines we see line up well with the Si IV absorption features from the host galaxy in the LBG composite of Shapley et al. (2003).

The Hainline et al. galaxies have continua presumably dominated by their host galaxies, which makes it intriguing that the ultraviolet spectral shape of the composite is similar to that of the class A composite. As Fig. 6 showed, the broad-band colours of our objects are similar to those of unobscured quasars. The continuum of the Shapley et al. (2003) LBG composite is significantly bluer than either of these samples, reflecting ongoing star formation in this ultraviolet-selected sample. Similarly, the star-forming galaxy at $z = 2.3$ studied by Erb et al. (2010) is much bluer than our composite. Hainline et al. (2012) point out that AGN spectral lines are strong in LBG spectra in the most luminous objects, which tend to be red; this is why the objects in their sample are redder than typical LBGs. In this interpretation, the similarity in continuum shape between our composite and that of Hainline et al. is fortuitous.

The comparison in the middle panel of Fig. 7 indicates that the relative strengths of emission lines in our objects and those of Hainline et al. (2011) are quite different. Following the emission-line diagnostic diagram of Villar-Martin, Tadhunter & Clark (1997), Fig. 8 compares the ratio of the strengths of C IV and He II to the ratio of C III] to C IV for our objects and those of Hainline et al. (2011), the compilation of narrow-line X-ray sources and radio galaxies of Nagao, Maiolino & Marconi (2006), the radio galaxies of De Breuck et al. (2000), the X-ray-selected type II quasar of Stern et al. (2002) and ultraviolet observations of the archetypal Seyfert II galaxy NGC 1068 (Kraemer & Crenshaw 2000). We also show the results for the class A and class B composites (red triangles), where we measure both the narrow components of the emission lines and the sum of narrow and broad components. The collisional excitation of C IV is sensitive to density and to gas temperature and thus metallicity. C IV can appear in emission in star-forming galaxies, although it is often swallowed by associated absorption in that line. However, the amount of C IV emission relative to other lines is much smaller in starbursts than in active nuclei. C III]/C IV depends on the relative abundance of these two ionization states of carbon, and thus this ratio is sensitive to the ionization parameter.

It is about 0.5 in active nuclei (Steidel et al. 2002), whereas it is 3 or greater in even the most extreme starbursts (Erb et al. 2010). Our objects fit squarely in the AGN regime; furthermore, we find that this ratio is considerably smaller for the narrow components of both class A and B composite spectra than for the full lines (Fig. 8). Similarly, He II may be produced in Wolf-Rayet stars or in extreme star formation regions with high-ionization parameters, a hard spectrum and low density, but this line has an equivalent width of no more than 2.7 \AA in starbursts (Erb et al. 2010), with only a handful of detections known. We detect He II in many individual spectra, and the equivalent width in the composite spectrum is about 6 \AA .

The ratio of C IV to He II is significantly higher, and the ratio of C III] to C IV lower, than in the other type II samples we have discussed (with the exception of NGC 1068). Indeed, the narrow-line region photoionization models of Groves, Dopita & Sutherland (2004) do not predict C IV/He II greater than 3 for any choice of their parameters, while the typical value for our sample is a ratio closer to 10. These high ratios are seen in broad-line regions; for example, the type I quasar composite spectrum of Vanden Berk et al. (2001) has C IV/He II ~ 50 , and the Seyfert I galaxy NGC 5448 (Korista & Goad 2000) has line ratios which place it in the middle of the cloud of class A objects in Fig. 8. So these narrow-line objects have line ratios like that of broad-line objects, but equivalent widths that are significantly higher. Indeed, our composite spectrum is like those of the ultraviolet spectrum of the Seyfert I spectrum NGC 5548 in its low state (Goad & Koratkar 1998), which shows narrow lines with broad bases, and emission-line ratios similar to our objects. An interesting possibility is that some of our objects may have similarly been observed spectroscopically in a low state; repeat spectroscopy and comparison of the photometry and spectrophotometry can test this hypothesis.

4.4 Associated absorption

The emission line widths have been measured by fitting Gaussian profiles to the spectra. However, the line profiles often differ significantly from Gaussian. A particularly dramatic example is shown in Fig. 9, where the Ly α and C IV lines show multiple peaks. This

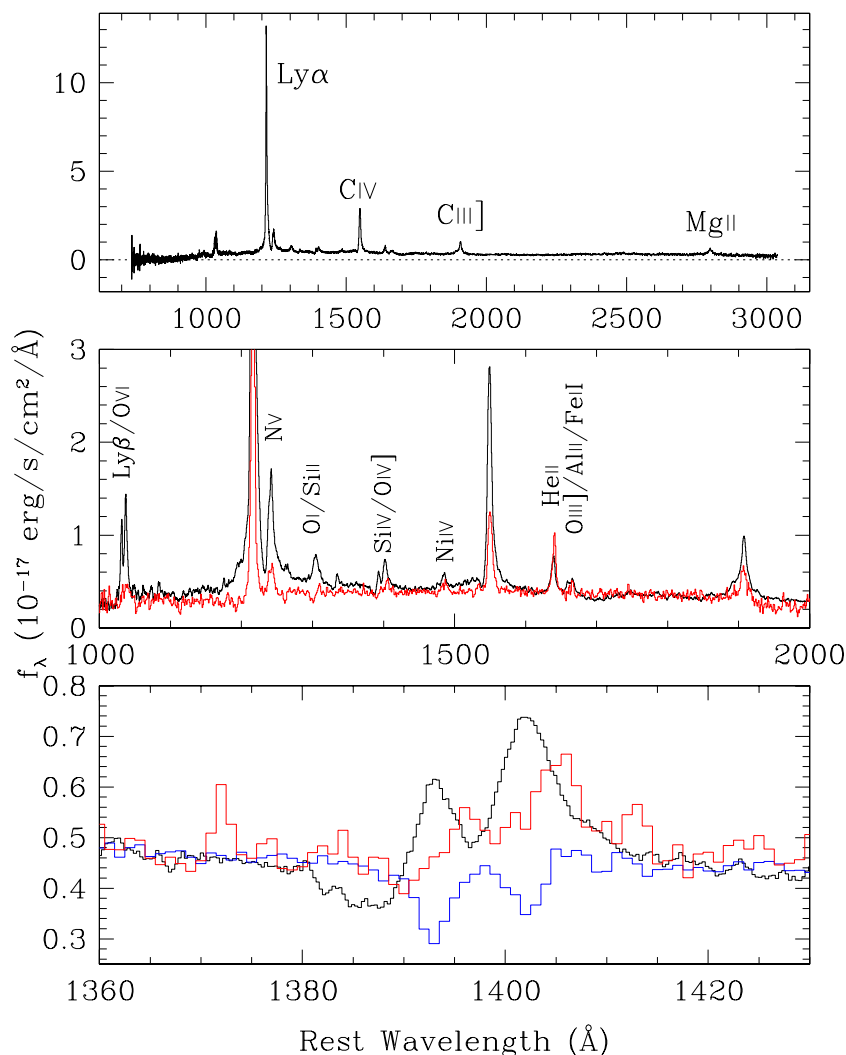


Figure 7. Upper: composite spectrum of all 145 class A type II quasar candidates; the dotted line is drawn at zero flux. Middle: an expanded view of the composite, to show the weaker emission lines. Note the absorption blueward of C IV and Si IV/O IV]. Superposed in red is the normalized composite of the Hainline et al. (2011) sample of high-redshift AGN, normalized to roughly match the continuum level at 1700 Å. The continuum slopes of the two composites are quite similar. The Ly α line in the Hainline et al. (2011) composite peaks at a flux density level half of that in the class A composite. Lower: an expansion of the composite in the region around the Si IV doublet. The black line represents our composite (lightly smoothed). The two emission features are the Si IV doublet at 1393.76 and 1402.77 Å, respectively; note the absorption trough blueward of it. The blue curve shows the composite LBG spectrum of Shapley et al. (2003, normalized to the same continuum); the absorption features precisely align with the emission lines in our composite. The red curve shows the composite spectrum of type II objects from Hainline et al. (2011). Intriguingly, the Si IV lines are redshifted relative to rest frame by about 800 km s⁻¹, perhaps due to systematic absorption on their blue wing.

is at first glance reminiscent of low-redshift type II objects possessing emission lines with two or more peaks, interpreted as multiple AGN or biconical outflows (e.g. Liu et al. 2010; Comerford et al. 2012). However, a more likely interpretation of these systems is that they are due to associated absorption within the host galaxy of the AGN; associated C IV absorption is seen in the spectra of quasars with velocity offsets as large as 12 000 km s⁻¹ (Nestor et al. 2008). Some of the absorption features in Fig. 9 match in Ly α and C IV, but inspection of the emission-line profiles of all the objects in our sample shows many more cases in which Ly α displays absorption and C IV does not, as expected in sufficiently low-ionization gas, perhaps from neighbouring galaxies. About 12 per cent of our class A objects possess significant absorption in one or both of these lines; it may be that higher S/N spectra at higher resolution would show more. A handful of objects show absorption in C IV and not Ly α , which may point to hot gas in which all the hydrogen is ionized.

5 SAMPLE PROPERTIES FROM RADIO TO X-RAY

We now turn to the properties of our objects revealed by data beyond the SDSS itself. We match the sample with radio data from the Faint Images of the Radio Sky (FIRST; Becker et al. 1995) survey in Section 5.1 and near-infrared data from the *Wide-Field Infrared Survey Explorer* (WISE; Wright et al. 2010) in Section 5.2. Several sources have also been serendipitously detected at 24 μ m by the *Spitzer Space Telescope* (Section 5.3). We also used NASA's High Energy Astrophysics Science Archive Research Center (HEASARC²) to search for serendipitous X-ray coverage from the *XMM-Newton*, *Chandra* and *ROSAT* facilities

² <http://heasarc.gsfc.nasa.gov>

Table 4. Measured emission-line fluxes from the composite spectra of our class A, class B and NLS1 samples. For strong emission lines where two components were fitted, we include values for both a narrow and broad component; see Table 5.

Emission line	Wavelength (Å)	Class A flux (10^{-17} erg s $^{-1}$ cm $^{-2}$)	Class B flux (10^{-17} erg s $^{-1}$ cm $^{-2}$)	NLS1 flux (10^{-17} erg s $^{-1}$ cm $^{-2}$)
Ly α (narrow)	1216	35.1	28.5	26.3
Ly α (broad)	1216	37.9	28.6	34.8
N v (narrow)	1240	3.4	3.2	4.4
N v (broad)	1240	9.7	12.3	22.8
[O I]	1305	1.8	1.2	1.3
C II	1337	0.24	0.22	0.24
Si IV	1397	0.34	0.4	1.0
O IV]	1402	1.9	1.4	1.9
N IV]	1486	0.76	0.25	0.13
C IV (narrow)	1549	10.5	9.3	10.8
C IV (broad)	1549	12.3	13.1	18.5
He II (narrow)	1638	1.8	1.2	1.4
He II (broad)	1638	0.8	1.6	2.5
[O III] + Al II + Fe II	1665	0.89	0.66	0.67
Al III	1857	0.24	0.33	0.60
Si III] + Fe III	1892	0.73	0.25	0.49
C III] + Fe III (narrow)	1906	1.4	1.8	2.1
C III] + Fe III (broad)	1906	6.7	6.4	9.7

Table 5. Measured emission line widths (FWHM) from the composite spectra. We include fits to two Gaussians, a narrow and broad component.

Emission line	Wavelength (Å)	Class A width (km s $^{-1}$)	Class B width (km s $^{-1}$)	NLS1 width (km s $^{-1}$)
Ly α (narrow)	1216	900	1040	1150
Ly α (broad)	1216	3130	3740	4140
C IV (narrow)	1549	1060	1220	1370
C IV (broad)	1549	3630	6170	7210

(Section 5.4). One of our sources is included in the Cosmic Evolution Survey (COSMOS) field (Scoville et al. 2007; Cappelluti et al. 2009) (Section 5.5). Finally, we present optical polarization data for two of our sources in Section 5.6.

5.1 Radio: Faint images of the Radio Sky at Twenty-cm

The FIRST survey (Becker et al. 1995) covers most of the SDSS footprint and was performed using the National Radio Astronomy Observatory (NRAO) Very Large Array (VLA) in its B-configuration in two channels at 1365 and 1435 MHz (~ 20 cm). Images were produced covering 1.8 arcsec pixel $^{-1}$ with an rms of

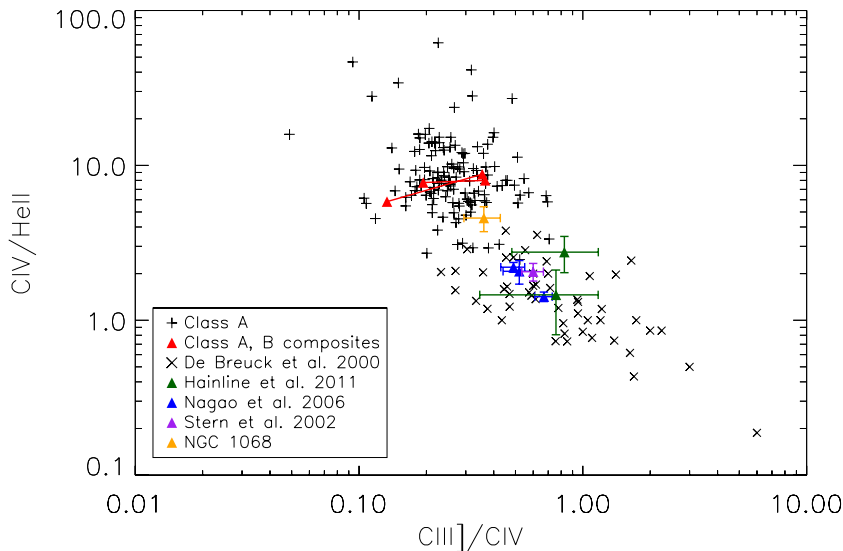


Figure 8. Comparison of C IV/He II and C III]/C IV for several samples of narrow-line AGN. The plus signs (+) indicate our class A candidates, and the red triangles are from the narrow components of the measured emission lines (left) and the broad+narrow emission lines (right, connected with a line) of our class A and class B composites. The green points indicate composites from the work of Hainline et al. (2011) where they split their population at a Ly α EW of 63 Å. The blue points are composites (X-ray-selected narrow-line quasars, low-redshift Seyfert IIs and high-redshift radio galaxies) from the compilation of Nagao et al. (2006) while the \times indicate high-redshift radio galaxies from De Breuck et al. (2000). We also show the *Chandra*-selected type II quasar at $z = 3.29$ of Stern et al. (2002), and ultraviolet observations of the low-redshift Seyfert II galaxy NGC 1068 (Kraemer & Crenshaw 2000).

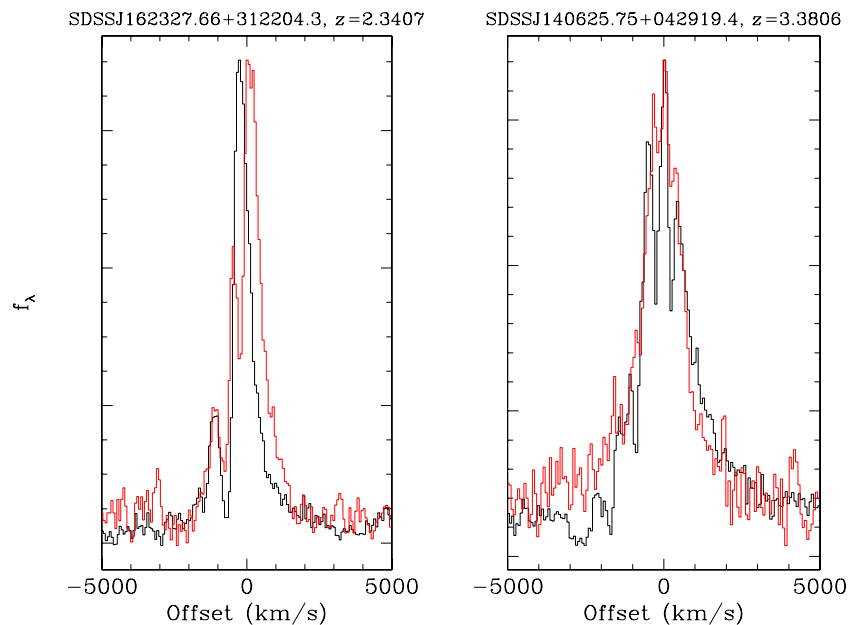


Figure 9. $\text{Ly}\alpha$ (black) and C IV (red) spectra for two class A objects, represented in velocity space. The two lines have been scaled to the same maximum. These objects have been chosen for their prominent associated absorption in these two lines. While the profiles of the two lines are similar, $\text{Ly}\alpha$ shows additional absorption features, suggestive of low-ionization gas. Some of the structure in the C IV line reflects the fact that it is a doublet. About 12 per cent of our class A objects show such associated absorption in their BOSS spectra.

Table 6. FIRST survey radio detections of class A and class B candidates.

Name	Peak flux (mJy beam $^{-1}$)	Integrated flux (mJy)
Class A		
SDSS J081257.252+181914.77	2.10	3.31 ± 0.146
SDSS J112343.182-010315.47	2.09	1.57 ± 0.154
SDSS J114753.301+3131 2.99	2.04	1.57 ± 0.278
Class B		
SDSS J005018.623+050132.50	1.28	0.81 ± 0.130
SDSS J013556.390-001631.83	1.02	0.93 ± 0.104
SDSS J093323.128-012307.61	1.13	1.13 ± 0.142
SDSS J133755.789+402150.20	1.15	0.97 ± 0.135
SDSS J144437.728-013625.50	5.68	5.33 ± 0.146
SDSS J145924.058+035622.40	3.31	3.07 ± 0.145
SDSS J160747.246+162123.67	3.43	3.17 ± 0.138
SDSS J161404.729+042122.83	10.21	9.89 ± 0.154
SDSS J163414.493+231737.47	3.38	3.40 ± 0.148

0.15 mJy and a resolution of 5 arcsec. Roughly 30 per cent of the FIRST sources have optical counterparts in SDSS imaging (Ivezić et al. 2002).

Radio-loud type II quasars are well studied at high redshift (McCarthy 1993); the typical high-redshift radio galaxy shows strong narrow emission lines reminiscent of the objects in our sample. There are only 12 objects in our sample of 452 class A and B candidates (less than 3 per cent) that match within 3 arcsec of a FIRST source;³ of these, only three are among the 145 class A candidates. These are listed in Table 6. However, the depth of the

FIRST survey is insufficient to designate an undetected object in our sample as radio quiet (Ivezić et al. 2002). Moreover, this classification depends on the ratio of optical to radio flux, and if the optical flux in our sources is significantly extinguished, the optical-to-radio ratio is meaningless. Indeed, while 8–20 per cent of all type I AGN are radio loud (Zakamska et al. 2004), only 1.5 per cent of type I quasars in the DR9 quasar catalogue with $21.5 < i < 22$ and redshifts between 2 and 3 are detected in the FIRST catalogue. The radio-loud fraction of type I quasars is lower at higher redshift (Jiang et al. 2007); it is possible that this also affects the number of radio detections in our sample.

Of the 12 matches, only one, SDSS J081257.15+181916.8, appears double-lobed in the FIRST images, with a separation between the lobes of roughly 10 arcsec, corresponding to a physical separation of about 80 kpc.

5.2 Mid-infrared: Wide-Field Infrared Survey Explorer (WISE)

WISE (Wright et al. 2010) observed the entire sky twice in four bands centred at 3.4, 4.6, 12 and 22 μm ($W1$, $W2$, $W3$ and $W4$) with 5σ sensitivity of 0.08, 0.11, 1 and 6 mJy and angular resolution 6.1, 6.4, 6.5 and 12.0 arcsec, respectively. At the typical redshift ($z = 2.5$) of our sample, the four WISE bands correspond to rest-frame 1, 1.3, 3.4 and 6.3 μm , respectively. Quasar SEDs show a break at $\sim 1 \mu\text{m}$, longwards of which hot dust can dominate the SED (e.g. Richards et al. 2006b), so only the relatively low-sensitivity $W3$ and $W4$ bands can tell us about dust emission in our objects.

Obscured quasars are expected to have a high ratio of rest-frame IR-to-optical emission. The IR light is produced by thermal emission of the obscuring material, so it should be present in both obscured and unobscured quasars, whereas the optical light is strongly suppressed in the latter. Unfortunately, the high redshifts of our candidates mean that WISE probes the rest-frame near-IR emission, which is not produced by the obscured material in large amounts and is thus not particularly strong in the SED of unobscured quasars

³ using the online catalogue at <http://sundog.stsci.edu/>.

Table 7. All WISE matches in our class A sample. Values are given in AB magnitudes.

SDSS name	W1	W1err	W2	W2err	W3	W3err	W4	W4err
SDSS0046+0005	19.77	0.19	18.92	0.22	16.57	Null	14.44	0.25
SDSS0146+1211	19.60	0.12	19.42	0.19	17.24	Null	15.28	Null
SDSS0154+0157	20.40	0.21	20.44	0.47	18.13	Null	15.63	Null
SDSS0206+0104	19.61	0.12	19.31	0.18	17.49	0.29	15.83	0.47
SDSS0232+0028	19.49	0.10	18.96	0.12	17.95	0.44	16.07	0.53

Only a portion of this table is shown here to demonstrate its form and content. A machine-readable version of the full table will be published online as Supporting Information.

Table 8. All WISE matches in our class B sample. Values are given in AB magnitudes.

SDSS name	W1	W1err	W2	W2err	W3	W3err	W4	W4err
SDSS0010+0003	19.46	0.15	18.70	0.13	17.38	0.35	15.39	0.51
SDSS0011-0008	19.29	0.12	19.67	0.34	17.51	0.45	15.10	Null
SDSS0201+0134	20.16	0.19	20.06	0.36	17.77	Null	15.38	Null
SDSS0232-0812	18.46	0.05	18.38	0.07	17.17	0.20	16.00	0.50
SDSS0234-0754	20.55	0.23	19.42	0.16	17.62	0.33	16.10	Null

Only a portion of this table is shown here to demonstrate its form and content. A machine-readable version of the full table will be published online as Supporting Information.

(Fig. 12). Furthermore, in obscured quasars the rest-frame near-IR may also be affected by extinction. The exception is the 22 μm band of *WISE*, which probes close to the peak of the infrared emission, but in most cases the *WISE* catalogue in this band is not sensitive enough for detecting our sources.

We accessed the *WISE* Source Catalog using the NASA/IPAC Infrared Science Archive (IRSA)⁴ and conducted a search within 2 arcsec of the positions of our class A and class B quasar candidates. 40 of our class A objects (27.6 per cent) and 62 (20.2 per cent) of our class B objects appeared in the *WISE* catalogue. While Wu et al. (2012) found that more than 85 per cent of optically bright quasars ($i < 19.5$) in DR7 had a *WISE* match, less than 50 per cent of those with $i > 20.5$ were matched, consistent with our result. While the *S/N* is typically low in bands *W3* and *W4* (due to the decreased sensitivity of these bands), 27 class A sources and 29 class B sources have an *S/N* above 5 in both bands *W1* and *W2* (only objects that were detected with an *S/N* > 5 in at least one band are included in the *WISE* All-Sky Release Catalog). All *WISE* sources are listed in Tables 7 and 8. *WISE* magnitudes are given on the AB system (Oke & Gunn 1983). Note that many errors are listed as ‘null’, indicating that the source is undetected in that band; the values listed represent 2σ upper limits on the flux.

There are only nine class A objects with *S/N* above 5 in *W3*, and only two in *W4*. Ross et al. (in preparation) will discuss the properties of the most extreme *W4* detections, with colours approaching those of the dust-obscured galaxy population discovered by Dey et al. (2008), among the SDSS and BOSS quasars. While none of these most extreme sources are among our type II quasar candidates, several of them show very weak continuum and broad emission lines. While their line widths are above our nominal 2000 km s^{-1} limit, their high IR-to-optical ratios suggest that they are obscured quasars. We will explore relaxing our rigid line-width criterion in future work.

Fig. 10 shows the *WISE* [3.6]–[4.5] colour of class A sources as a function of redshift; a sample of DR9 BOSS quasars with similar

i-band magnitudes is included for comparison. The colours of both samples become bluer at redshift $z \sim 3.5$, when $\text{H}\alpha$ enters the *W1* band (although this redshift range is not shown in Fig. 10). A K-S test says that the colour distributions of the two are the same at the 99.99 per cent level for those objects with redshift less than 3.5; there is no evidence that the type II objects are redder in this colour than unobscured quasars of similar brightness.

Similarly, Fig. 11 measures a colour between the SDSS and *WISE* bands. A K-S test shows that the colour distributions are the same at the 99.9 per cent confidence level. Much of the scatter in this diagram and Fig. 10 is due to measurement errors both in SDSS and *WISE*; these detections are often near the flux limit of both surveys.

5.3 Mid-infrared: *Spitzer* MIPS-24

Only a handful of objects are detected in the long wavelength filters of *WISE*. In order to obtain an independent estimate of the bolometric luminosities of our sources, we have searched the *Spitzer* Space Telescope archive for serendipitous coverage of our class A and class B samples. Using the *Spitzer* Heritage Archive,⁵ we searched for Multiband Imaging Photometer (MIPS; Rieke et al. 2004) 24 μm data covering the positions of our class A and class B sources. MIPS-24 is fairly close to the peak of the SED for normal unobscured quasars, whereas serendipitous MIPS observations at longer wavelengths (70 and 160 μm) are too shallow to yield any detections of our sources.

We found 13 sources that are covered by MIPS-24 observations. Several objects are covered by multiple exposures, which we co-added to increase the effective exposure time at the positions of our targets. We then conducted aperture photometry at the SDSS positions (accurate to 0.1 arcsec; Pier et al. 2003), using a circular aperture with a radius of 12 arcsec and a background annulus between 12 and 18 arcsec.

The photometric measurements are presented in Table 9. Five out of 13 sources are detected at the 4σ level or greater; another

⁴ <http://irsa.ipac.caltech.edu/cgi-bin/Gator/nph-dd>

⁵ <http://sha.ipac.caltech.edu/applications/Spitzer/SHA/>

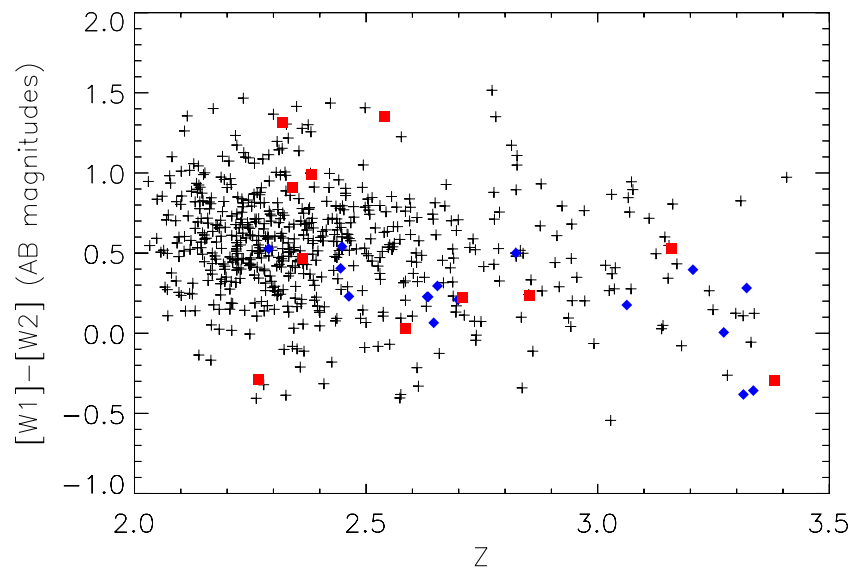


Figure 10. *WISE* colour ($W1-W2$, i.e. $[3.4]-[4.6]$) as a function of redshift for candidate type II quasars below redshift 3.5; red squares are those objects detected above 5σ in both bands, while the blue diamonds are sources detected below 5σ in one or both bands. The grey crosses are a sample of type I quasars from DR9 with a similar distribution of i -band magnitude with *WISE* detections, and thus similar photometric errors. The distribution of colours is indistinguishable between the two samples with a K-S test.

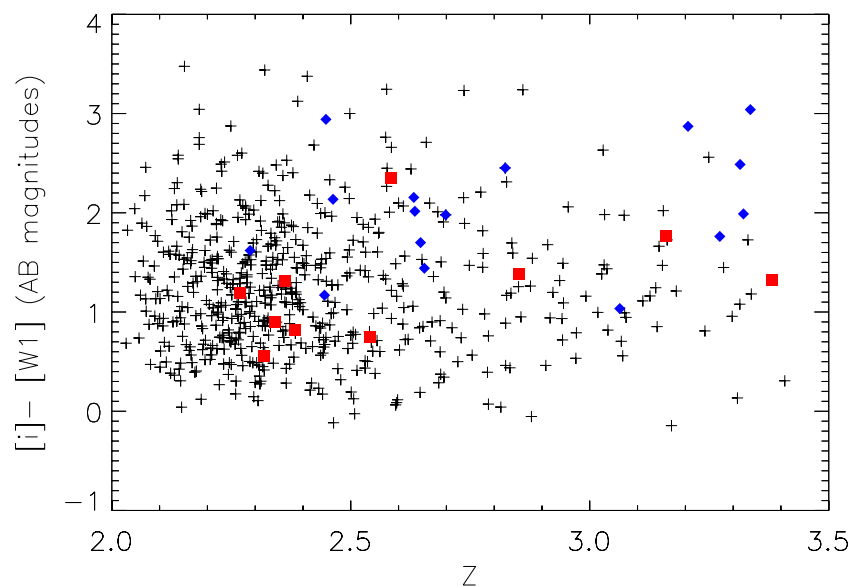


Figure 11. The colour of type II candidates between the SDSS i and $W1$ bands, as a function of redshift; symbols are as in Fig. 10. The distributions of colours of the type II and type I samples are indistinguishable with a K-S test.

four sources are marginally detected. We used the observed *Spitzer* fluxes to calculate the rest-frame monochromatic luminosity at $6\ \mu\text{m}$. At the redshifts of our detected sources, an observed wavelength of $24\ \mu\text{m}$ corresponds to rest-frame $5.9-7.3\ \mu\text{m}$; we k -correct to $6\ \mu\text{m}$ using $F_\nu \propto \nu^{-1.09}$ from the average type I SED by Richards et al. (2006b). The bolometric luminosities of our objects can be estimated by multiplying the monochromatic luminosities at $6\ \mu\text{m}$ by a factor of 8, again taken from Richards et al. (2006b).

Thus, approximately half of the objects covered by the MIPS-24 data are detected at the level $0.5-1\ \text{mJy}$, with detection luminosities in the range $\nu L_\nu[6\ \mu\text{m}] = 10^{45.4-45.9}\ \text{erg s}^{-1}$ and estimated bolometric luminosities $10^{46.3-46.8}\ \text{erg s}^{-1}$. Thus, these objects are indeed very luminous quasars.

5.4 X-Ray: *XMM-Newton*, *Chandra* and *ROSAT*

Luminous X-ray emission is nearly ubiquitous in unobscured quasars (e.g. Mushotzky 2004; Gibson, Brandt & Schneider 2008), and high-quality X-ray spectra of these type II quasar candidates could usefully constrain their obscuration levels and/or intrinsic luminosities (e.g. Brandt & Hasinger 2005; Vignali et al. 2010; Alexander et al. 2011; Comastri et al. 2011; Jia et al. 2012). We therefore have searched the *Chandra*, *ROSAT* and *XMM-Newton* archives for sensitive X-ray coverage of the sources in our sample. Sources having sensitive X-ray coverage were individually inspected in X-ray and SDSS images to assess critically the reliability of putative X-ray detections and X-ray/SDSS associations. This screening identified five X-ray detected objects and another

Table 9. *Spitzer* 24 μ m data.

Object	Flux density (mJy)	Class	$\log(\nu L\nu/(\text{ergs}^{-1}))$ (6 μ m)
Detections:			
SDSS J095819.35+013530.5	0.76 ± 0.10	A	45.89
SDSS J010554.41+011326.9	0.85 ± 0.16	B	45.94
SDSS J122353.62+050321.0	1.01 ± 0.12	B	45.77
SDSS J135136.57+381642.8	0.42 ± 0.11	B	45.39
SDSS J142610.76+341738.9	1.07 ± 0.12	B	45.72
Marginal detections and non-detections:			
SDSS J021834.53-033518.5	0.21 ± 0.06	A	
SDSS J161447.98+354221.2	-0.11 ± 0.14	A	
SDSS J020546.33+013907.6	-0.10 ± 0.14	B	
SDSS J022429.14-024807.7	-0.28 ± 0.08	B	
SDSS J115840.06+014335.3	0.15 ± 0.06	B	
SDSS J121326.70+062922.8	0.24 ± 0.07	B	
SDSS J124219.55+413720.6	0.21 ± 0.08	B	
SDSS J141649.80+365012.2	0.87 ± 1.04	B	

Table 10. X-Ray detections of type II quasar candidates by *Chandra*, *ROSAT* and *XMM-Newton*.

SDSS coordinate	Facility	Observation ID	Screened effective exposure (ks)	Energy band (keV)	Observed flux (10^{-15} erg s^{-1} cm^{-2})	Notes
014841.83+055024.19	<i>XMM-Newton</i>	0112551501	10.6	0.2–12	16	2XMM
082726.58+262803.00	<i>XMM-Newton</i>	0103260601	11.1	0.2–12	23	2XMM
082726.76+214557.08	<i>Chandra</i>	10268	10.0	0.3–8	31	
095819.35+013530.52	<i>XMM-Newton</i>	0302353301	6.3	0.2–12	24	2XMM
142610.77+341738.85	<i>Chandra</i>	7388	4.5	0.5–8	4.8	¹
160554.89+202729.87	<i>ROSAT</i>	rp600588n00	16.1	0.5–2	8.6	²

Three of the sources are included in the second *XMM-Newton* serendipitous source catalogue (2XMM; Watson et al. 2009). The screened effective exposure time corrects for the effects of vignetting and for time lost to flares.

¹Two-photon detection; in NAO Deep Wide-Field Survey Bootes field,

²*ROSAT* identification likely correct but needs verification.

that is likely X-ray detected (SDSS J160554.89+202729.87); the X-ray properties of these sources are listed in Table 10. All of these sources were serendipitous detections rather than the targets of their respective observations. In addition, five sources (SDSS J023337.89+002303.69, SDSS J023359.27+005925.83, SDSS J120355.19+014348.98, SDSS J144227.31-004725.04 and SDSS J144441.05-001343.44) are undetected in X-rays in observations of generally comparable sensitivity to those that yielded the detections in Table 10.

The sources with X-ray detections in Table 10 have 2–99 counts; five of the six sources have 45 or fewer counts. Most also have high backgrounds in the source detection cell owing to large off-axis angles. Thus, unfortunately, none of these sources has sufficient S/N for useful X-ray spectroscopy that could constrain, via X-ray spectral shape, absorption and intrinsic luminosity. Additional X-ray observations are required to perform such spectroscopy. Alternatively, once independent multiwavelength luminosity indicators are available for these sources (e.g. [O III] 5008 Å and far-infrared luminosities), these can be correlated with even basic X-ray emission measurements to assess obscuration levels (e.g. Vignali et al. 2010; Jia et al. 2012).

5.5 Cosmic Evolution Survey

The COSMOS⁶ covered 2 deg² with the *Hubble Space Telescope* (*HST*) Advanced Camera for Surveys (ACS; Koekemoer et al.

2007), the VLA (Schinnerer et al. 2004), the *Spitzer Space Telescope* (Sanders et al. 2007), *XMM-Newton* (Hasinger et al. 2007) and other facilities. One of our sources, SDSS J095819.35+013530.5 at $z = 3.0554$ (hereafter SDSS0958+0135), lies in the COSMOS field. This object therefore has extensive multiwavelength coverage and an exquisitely measured SED. The optical and NIR photometry from 15 bands is available via the IRSA, and so is the *Spitzer* Infrared Array Camera (IRAC) (3.6–8 μ m) and MIPS-24 μ m photometry (as we saw in Section 5.3). The source is not in the MIPS-70 μ m catalogue of COSMOS. We co-added all 14 available MIPS-70 μ m exposures, conducted aperture photometry and obtained a tentative detection with a flux of 1.13 ± 0.7 mJy.

In Fig. 12, we use multiband data from the COSMOS survey to construct the SED of this object and compare it with those of a type I quasar template from Richards et al. (2006b) and a type II (obscured) quasar template derived from *Spitzer* data (Zakamska et al. 2008) of low-redshift luminous optically selected obscured quasars (Zakamska et al. 2003). The templates have been arbitrarily normalized to match the observed SED at rest-frame 6 μ m (as measured by MIPS-24 μ m).

The SED of SDSS0958+0135 shows several noteworthy features. The ultraviolet to infrared flux ratio is significantly lower than in unobscured quasars (and the high equivalent width of Ly α in emission contributes significantly to the ultraviolet flux). However, the ultraviolet emission in this source is not as suppressed as it is in low-redshift obscured quasars. This feature suggests that SDSS0958+0135 is reddened by moderate amounts of dust, perhaps in its host galaxy. Extinction with $A_V = 0.3$ –0.6 mag would suppress the ultraviolet continuum by a factor of 3, but would leave

⁶ <http://cosmos.astro.caltech.edu/index.html>

longer wavelengths much less affected. Another possibility is that the object is strongly absorbed, and the observed continuum in the ultraviolet is produced by quasar light that is scattered off the material in the host galaxy and reaches the observer, even though the central engine itself is not visible along our line of sight. However, matching the observed optical SED would require ~ 10 per cent scattering efficiency, which is quite extreme. Future polarization measurements of the kind discussed in the next section will help distinguish these two possibilities.

The SED of SDSS0958+0135 appears to peak at relatively short wavelengths – around rest-frame $6\ \mu\text{m}$ – declining to longer wavelength, which is similar to the shape of the SED of unobscured quasars, and unlike low-redshift obscured quasars whose SEDs tend to show more cold dust emission. The shape of the mid-infrared SED is consistent with that of a reddened quasar, since modest amounts of reddening applied to a type I spectrum would not affect mid-infrared wavelengths. Another possibility is a strongly obscured source, but with a compact and hot obscuring region rather than an extended colder one. The observed MIPS-24 flux of $0.76\ \text{mJy}$ corresponds to a monochromatic luminosity of $\nu L_\nu[6\ \mu\text{m}] = 7.7 \times 10^{45}\ \text{erg s}^{-1}$, as we saw in Section 5.3. The similarity of the mid-infrared SED of SDSS0958+0135 to that of type I quasars enables us to use bolometric corrections derived by Richards et al. (2006b, a factor of 8 at this wavelength), leading to $L_{\text{bol}} = 6 \times 10^{46}\ \text{erg s}^{-1}$ in this source. This is clearly a very luminous quasar.

As part of the COSMOS survey, this source was observed in the $0.5\text{--}2\ \text{keV}$ band by *XMM-Newton*; the inferred luminosity in the $2\text{--}8\ \text{keV}$ rest frame is $9.2 \times 10^{43}\ \text{erg s}^{-1}$ (not shown in Fig. 12). This object was also observed by the *Hubble Space Telescope* in the ACS/F814W filter, just redward of the $\text{Ly}\alpha$ emission, for a full orbit (2028 s on-source). The object is unresolved in the *HST* image; neither the emission from the host galaxy nor extended scattered light are detected. At this redshift, $0.1\ \text{arcsec}$, a reasonable upper

limit on the size of the object in the ACS data, corresponds to a physical extent of roughly $1\ \text{kpc}$, suggesting a very compact object indeed. This is not surprising if the light is dominated by the direct (albeit reddened) light from the quasar itself. If, on the other hand, the object is a highly obscured quasar, then the limit on the size of the rest-frame ultraviolet emission suggests that the scattering interstellar medium in the host galaxy is compact. This model would be consistent with recent findings that massive galaxies at high redshifts tend to have small effective sizes (Wuyts et al. 2010).

5.6 Optical polarization

Optical polarimetry is a classical test of the obscuration-based unification model of AGN (Antonucci & Miller 1985). Even if the direct line of sight to the nucleus is blocked by obscuration, quasar light can escape along an unobscured direction (or sometimes more than one; Schmidt et al. 2007), scatter off free electrons or dust particles in the interstellar medium of the host galaxy and reach the observer. Since scattered light is polarized, optical polarimetry and spectropolarimetry are uniquely sensitive to the scattered component.

This process occurs both in obscured and unobscured quasars, but in the latter the scattered component is diluted by the emission from the quasar itself, so the typical levels of polarization in unobscured quasars is 0.5 per cent (Berriman et al. 1990). In obscured or heavily reddened quasars with large enough column density along the line of sight, the scattered component dominates over the direct emission, and the typical levels of polarization are much higher – a few per cent (Tran 1995; Smith et al. 2002, 2003; Zakamska et al. 2005), reaching $\gtrsim 20$ per cent in several exceptional cases (Hines et al. 1995; Smith et al. 2000; Zakamska et al. 2005). Thus, high levels of polarization are strongly suggestive of an obscured active nucleus. The spectrum of the polarized component can be that of

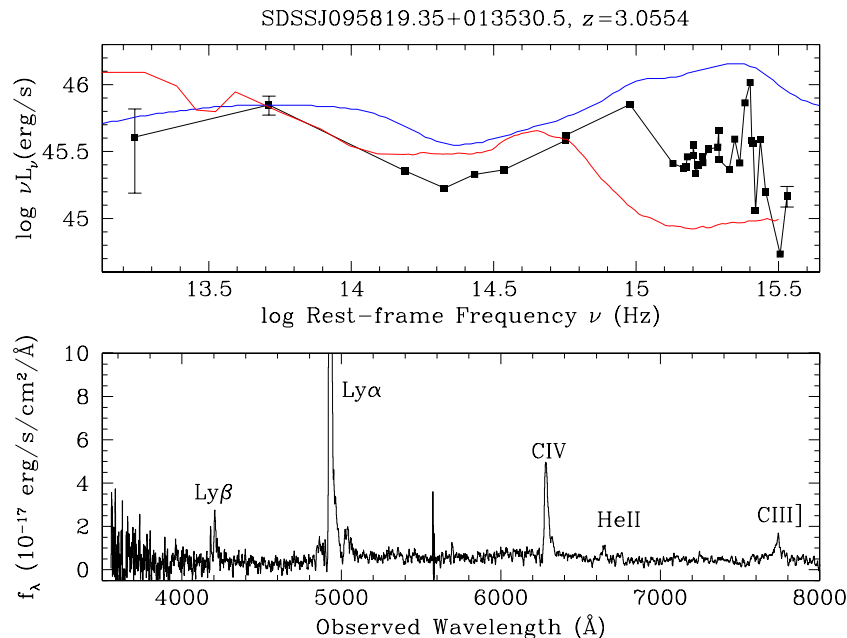


Figure 12. Upper: the SED of SDSS0958+0135, which lies in the COSMOS field, including data from the *Spitzer Space Telescope* and a variety of ground-based facilities. The peak at $\log \nu = 15.4$ is due to $\text{Ly}\alpha$ emission. For comparison, the blue line is the composite type I SED from Richards et al. (2006b) and the red line is the mean low-redshift type II quasar SED (Zakamska et al. 2008). All curves are normalized to a rest-frame frequency of $10^{13.7}\ \text{Hz}$ ($6\ \mu\text{m}$, corresponding to the $24\ \mu\text{m}$ detection with *Spitzer*). Lower: the BOSS spectrum of this source with expanded vertical and horizontal axes (the peak of the $\text{Ly}\alpha$ line is well off-scale), with emission lines marked. The C IV line is markedly asymmetric, perhaps indicating self-absorption on the blue side.

an unobscured quasar, showing a blue continuum and broad permitted emission lines (Antonucci & Miller 1985; Zakamska et al. 2005).

In 2012 September, we observed two high-redshift type II quasar candidates from our class A sample with the CCD Spectropolarimeter (SPOL; Schmidt, Stockman & Smith 1992) on the 6.5 m MMT using the National Optical Astronomical Observatory time allocation in suboptimal weather conditions. SDSS J220126.11+001231.5 was observed over 4 h, and SDSS J004728.77+004020.3 over 2 h, with a 1.1 arcsec slit and low-resolution grating, resulting in wavelength coverage of 4000–8000 Å and spectral resolution 19 Å. Because the sources are faint ($i = 20.7$ and $i = 21.2$ mag, respectively), we bin the data in wavelength, allocating bins separately for continuum-dominated and emission-line-dominated regions. The combined results of the MMT observations are shown in Fig. 13. Unfortunately, this binning and the limited S/N mean that we are not able to measure the width of the lines in polarized light.

When averaged over the high S/N continuum region of 5000–7000 Å, SDSS2201+0012 is polarized at a level of 1.9 ± 0.3 per cent, with position angle $176^\circ \pm 4^\circ$ (east of north). This polarization is significantly higher than the typical polarization of unobscured quasars (0.5 per cent), any instrumental systematics ($\lesssim 0.1$ per cent), or polarization that can be acquired due to the propagation of light through the dust in the Galaxy (< 0.8 per cent; Berriman et al. 1990). There is no evidence that the narrow emission lines are polarized any less than the surrounding continuum, indicating that the scattering medium is distributed on scales that are larger than the narrow-line region. For the COSMOS source (Section 5.5), we concluded that the scattering region had to be compact; additional spectrophotometry and high-resolution imaging of the same sources (Zakamska et al. 2006) will be valuable to determine whether there is a contradiction here.

The polarization fraction rises towards the blue part of the spectrum, where it reaches > 5 per cent. This change is either indicative of a wavelength-dependent scattering mechanism or of a red unpolarized component that dilutes blue polarized light (Zakamska et al. 2005). Since electrons scatter optical and UV light in a wavelength-independent manner, the first possibility calls for dust particles to be primarily responsible for scattering. This is not an uncommon occurrence, especially in high-luminosity obscured or reddened quasars where scattering occurs over a large fraction of the entire host galaxy (Hines et al. 2001; Zakamska et al. 2005; Schmidt et al. 2007) rather than being confined to the highly ionized circumnuclear material (Antonucci & Miller 1985). However, the contribution of the unpolarized but reddened quasar continuum can mimic the wavelength dependence of the polarized fraction, and we cannot rule out either of these explanations with the current data. Rest-frame optical (observed-frame near-infrared) observations will help distinguish these scenarios by allowing us to determine the shape of the continuum and thus the level of quasar obscuration. The high S/N MMT spectrum reveals a hint of a broad shallow absorption feature blueward of C IV, which is thought to come from the central region in AGN, suggesting that the light from the central engine is not completely obscured. In any case, the high level of polarization seen in SDSS2201+0012 strongly suggests that it is either an obscured or a heavily reddened quasar.

SDSS0047+0040 is not as highly polarized as SDSS2201+0012, with an average polarization over 5000 to 7000 Å of 0.91 ± 0.35 per cent (position angle $28^\circ \pm 10^\circ$). The most striking feature in this source is that the mini-absorption trough blueward of the C IV emission line is polarized at a level of ~ 6 per cent, or $> 3\sigma$ higher than the continuum. This feature is similar to that seen in BAL quasars (e.g. DiPompeo, Brotherton & De Breuck 2011). Indeed, in these sources the absorption trough blocks the direct light from the quasar and thus suppresses the quasar continuum

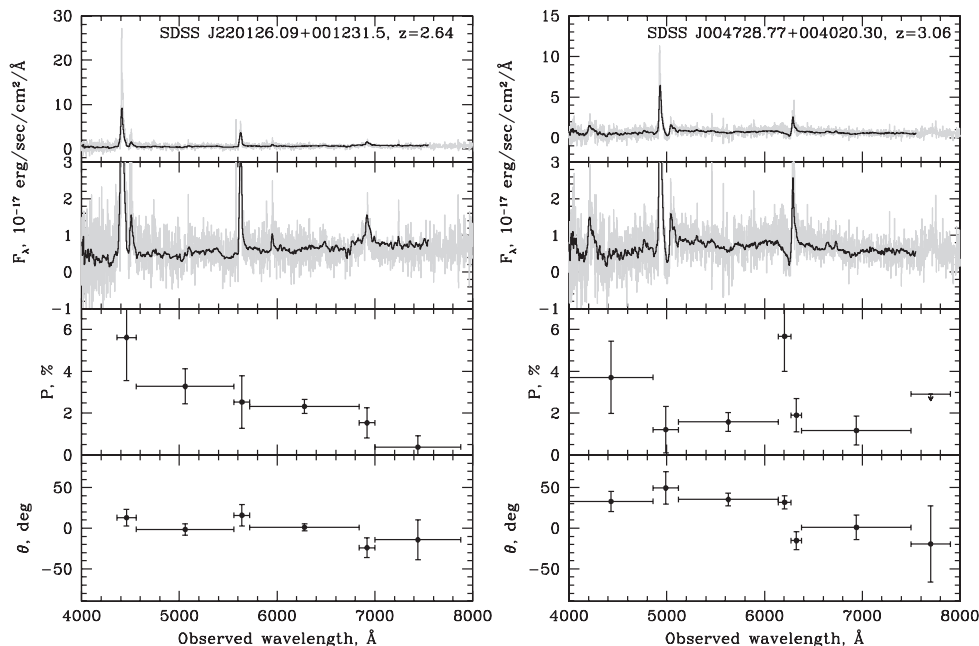


Figure 13. Results of spectropolarimetric observations of two candidate obscured quasars with SPOL on MMT. In the top panels, we show the BOSS spectra in grey and MMT spectra in black (both the overall spectra and an expanded view to highlight weak features are shown). The MMT spectra were taken in non-photometric conditions and have been scaled up by a factor ~ 1.5 to line up with the SDSS continuum. In the bottom panels, we show the fractional polarization measured using SPOL observations, in per cent, and the polarization position angle in degrees E of N. These have been binned over interesting wavelength regions (continuum and lines) to build up S/N.

contribution relative to the scattered light emission produced on larger spatial scales, increasing the level of polarization seen within the trough relative to that seen at other wavelengths. We conclude that the modest level of polarization of SDSS0047+0040 and the polarization increase within the mini-trough suggest that some of the continuum in this source is direct quasar light. The definitive test to determine whether these two objects are obscured would be broad emission lines in the polarized spectrum. This will require substantially higher S/N spectropolarimetry than we have obtained.

6 DISCUSSION

We consider our objects to be candidate type II quasars by drawing an analogy with the defining characteristics of Seyfert II galaxies at lower redshift: narrow permitted lines seen in the rest-frame ultraviolet, and a relatively weak continuum, as quantified by high equivalent widths of these lines. The key questions, which we have yet to answer, are: (a) what are the intrinsic luminosities of these objects; and (b) what is the range of the obscuration we probe in this sample. We do know that at least some of these sources are highly luminous ($>10^{46}$ erg s $^{-1}$), given detections in the *Spitzer* MIPS-24 μ m band (Section 5.3). Although *WISE* data do not go out to long enough wavelengths to probe the peak of the IR SED, they indicate similarly high luminosities for a few other sources in this sample. X-rays are another probe of unobscured luminosity; observations in the 2–10 keV energy range sample rest-frame energies from 7 to 35 keV, where even moderately Compton-thick sources should be detected. We have serendipitous detections of a handful of sources (Section 5.4), but targeted observations with *Chandra* or *XMM-Newton* will yield new insights into their true luminosities.

Our objects have continuum absolute magnitudes of -23 and brighter in the ultraviolet (Fig. 5); this is too luminous to be explained by the stellar continuum of the host galaxy of an obscured quasar. Indeed, the brightest unenslaved galaxies known at $z > 2$ are roughly $r = 24$ (Shapley 2011), two magnitudes fainter than the faintest objects in our sample. Thus, the continuum light that we are seeing must be dominated by the nucleus itself. There are three possible explanations: (a) these sources are only modestly extinguished ($A_V \sim 0.5$, corresponding to 1.5 mag of extinction at 1500 Å for an $R = 3.1$ extinction law), (b) substantial amounts of quasar continuum light are scattered by distributed dust or electrons, as is seen in lower redshift type II quasars or (c) the line of sight to the central region is heavily obscured, but the covering fraction is not complete, allowing some amount of unobscured continuum through. The relatively blue continuum and the broad bases seen on the emission lines in the composite spectrum (Fig. 7) are consistent with all three of these hypotheses, and the rough similarities in the broad-band colours and SEDs of these objects and type I objects are supportive of the scattering and partial covering hypotheses. We have polarization data on only two objects to date (Section 5.6); the fact that both objects are strongly polarized suggests extinguished objects with substantial scattering. It may well be that our sample is heterogeneous, with some more extinguished than others. With this in mind, it is dangerous to draw conclusions about the whole population from just a few objects.

Lower redshift obscured quasars have been identified as such by their narrow Balmer emission lines. Near-infrared spectroscopy allows measurement of these lines directly in our high-redshift objects, to determine whether the permitted lines remain narrow at wavelengths where extinction due to dust is significantly smaller. We will report observations in the near-infrared in a paper in preparation; consistent with the modest extinction hypothesis, many of

our sources do show evidence for broad Balmer lines. The near-infrared data will also allow us to measure the luminosity in the [O III]5008 Å emission line, which has been used as a proxy for bolometric luminosity.

If the continua in these objects include a contribution from scattering, we might detect extended scattered emission in high-resolution images, as is seen in lower redshift type II quasars (Zakamska et al. 2006). The COSMOS object is unresolved in *HST* images, but we have an ongoing *HST* programme to image six sources from our survey; the results will be presented in a future paper.

If the continuum we are seeing from these objects is dominated by scattered light on kpc scales, one would not expect to see variability on human time-scales. A number of our objects fall on the Equatorial Fall Stripe in the Southern Galactic Cap ('Stripe 82'), which was repeatedly imaged during the SDSS (Abazajian et al. 2009), allowing a search for such variability.

In future work, we hope to use this sample to quantify the relative numbers of obscured and unobscured quasars as a function of redshift and luminosity. This is a challenging task, given the uncertainties we have just discussed about the amount of extinction and the true luminosities of our sources. However, these objects are not extremely rare: the 145 sources in our class A sample are drawn from SDSS DR9, which represents only the first year of BOSS data taking, or about 1/3 of the final BOSS survey. We can expect the sample to triple in size by the time of the final BOSS data release in late 2014. Future wide-angle spectroscopic surveys on larger telescopes, such as those to be carried out by the Prime Focus Spectrograph being built for the Subaru Telescope (Takada et al. 2012), may reveal substantially more such objects.

7 CONCLUSIONS

We have identified a sample of candidate type II quasars at redshifts between 2.0 and 4.3 from the spectra of the BOSS. They are characterized by strong narrow (FWHM < 2000 km s $^{-1}$) Ly α and C IV emission lines of high equivalent width. Our sample includes 145 'class A' objects, plus an additional 307 'class B' objects whose classification is less certain. Our main conclusions are as follows.

- (i) These objects have continuum absolute magnitudes of -23 and brighter, suggesting that the quasar continuum is only modestly extinguished, that the extinction is patchy or that the quasar continuum is strongly scattered.
- (ii) A composite high S/N spectrum shows broad bases (FWHM ~ 3500 km s $^{-1}$) in many emission lines, suggesting modest extinction or substantial scattering of light from the central engine.
- (iii) The distribution of broad-band colours of these objects from the rest-frame ultraviolet to 1 μ m are consistent with those of unobscured quasars at the same redshift.
- (iv) The ratios of the strengths of the C IV, He II and C III] emission lines are distinctly different from those of other classes of type II AGN at high redshift, suggesting a higher ionization parameter and a lower metallicity than these other samples.
- (v) Many of the objects show significant self-absorption in the Ly α and C IV emission lines, often blueshifted relative to the rest-frame peaks of the lines, suggesting substantial absorbing gas and outflows.
- (vi) Serendipitous observations of a dozen objects at 24 μ m with the *Spitzer Space Telescope* imply bolometric luminosities above 10^{46} erg s $^{-1}$.
- (vii) Polarization measurements of two objects suggest that there is a significant scattered component to the continuum.

(viii) Further insights into the intrinsic luminosities, obscuration and physical nature of these sources will require additional X-ray, near- and mid-infrared, and spectropolarimetric observations.

ACKNOWLEDGEMENTS

We thank Kevin Hainline and Dan Stern for useful discussions and the use of their spectra, and Gordon Richards and Joe Hennawi for useful comments on an early draft of the paper.

Funding for SDSS-III has been provided by the Alfred P. Sloan Foundation, the Participating Institutions, the National Science Foundation and the US Department of Energy Office of Science. The SDSS-III website is <http://www.sdss3.org/>.

SDSS-III is managed by the Astrophysical Research Consortium for the Participating Institutions of the SDSS-III Collaboration including the University of Arizona, the Brazilian Participation Group, Brookhaven National Laboratory, University of Cambridge, Carnegie Mellon University, University of Florida, the French Participation Group, the German Participation Group, Harvard University, the Instituto de Astrofísica de Canarias, the Michigan State/Notre Dame/JINA Participation Group, Johns Hopkins University, Lawrence Berkeley National Laboratory, Max Planck Institute for Astrophysics, Max Planck Institute for Extraterrestrial Physics, New Mexico State University, New York University, Ohio State University, Pennsylvania State University, University of Portsmouth, Princeton University, the Spanish Participation Group, University of Tokyo, University of Utah, Vanderbilt University, University of Virginia, University of Washington and Yale University. RA and MAS acknowledge the support of NSF grant AST-0707266, and JEG and NZ acknowledge the support of Alfred P. Sloan Foundation Fellowships. NZ is also supported by the Theodore Dunham, Jr, Grant of the Fund for Astrophysical Research. WNB acknowledges the support of NASA ADAP grant NNX10AC99G and NSF grant AST-1108604.

This publication makes use of data products from the Wide-field Infrared Survey Explorer, which is a joint project of the University of California, Los Angeles, and the Jet Propulsion Laboratory/California Institute of Technology, funded by the National Aeronautics and Space Administration. This research has made use of the NASA/IPAC IRSA, which is operated by the Jet Propulsion Laboratory, California Institute of Technology, under contract with the National Aeronautics and Space Administration. This research has made use of data obtained from the High Energy Astrophysics Science Archive Research Center (HEASARC), provided by NASA's Goddard Space Flight Center.

REFERENCES

Abazajian K. N. et al., 2009, *ApJS*, 182, 543
 Ahn C. P. et al., 2012, *ApJS*, 203, 21
 Alexander D. M., Smail I., Bauer F. E., Chapman S. C., Blain A. W., Brandt W. N., Ivison R. J., 2005, *Nat*, 434, 738
 Alexander D. M. et al., 2011, *ApJ*, 738, 44
 Anderson L. et al., 2012, *MNRAS*, 427, 3435
 Antonucci R., 1993, *ARA&A*, 31, 473
 Antonucci R. R. J., Miller J. S., 1985, *ApJ*, 297, 621
 Assef R. J. et al., 2013, *ApJ*, 772, 26
 Ballantyne D. R., Draper A. R., Madsen K. K., Rigby J. R., Treister E., 2011, *ApJ*, 736, 56
 Barger A. J., Cowie L. L., Mushotzky R. F., Wang W.-H., Steffen A. T., Capak P., 2005, *AJ*, 129, 578
 Becker R. H., White R. L., Helfand D. J., 1995, *ApJ*, 450, 559
 Bentz M. C., Hall P. B., Osmer P. S., 2004, *AJ*, 128, 561

Berriman G., Schmidt G. D., West S. C., Stockman H. S., 1990, *ApJS*, 74, 869
 Bolton A. S. et al., 2012, *AJ*, 144, 144
 Bovy J. et al., 2011, *ApJ*, 729, 141
 Brandt W. N., Hasinger G., 2005, *ARA&A*, 43, 827
 Busca N. G. et al., 2013, *A&A*, 552, A96
 Canalizo G., Stockton A., 2001, *ApJ*, 555, 719
 Cappelluti N. et al., 2009, *A&A*, 497, 635
 Civano F. et al., 2012, *ApJS*, 201, 30
 Comastri A. et al., 2011, *A&A*, 526, L9
 Comerford J. M., Gerke B. F., Stern D., Cooper M. C., Weiner B. J., Newman J. A., Madsen K., Barrows R. S., 2012, *ApJ*, 753, 42
 Constantin A., Shields J. C., 2003, *PASP*, 115, 592
 Coppin K. et al., 2010, *ApJ*, 713, 503
 Dawson K. S. et al., 2013, *AJ*, 145, 10
 De Breuck C., Röttgering H., Miley G., van Breugel W., Best P., 2000, *A&A*, 362, 519
 Dey A. et al., 2008, *ApJ*, 677, 943
 DiPompeo M. A., Brotherton M. S., De Breuck C., 2011, *ApJS*, 193, 9
 Donley J. L. et al., 2012, *ApJ*, 748, 142
 Eisenstein D. J. et al., 2011, *AJ*, 142, 72
 Erb D. K., Pettini M., Shapley A. E., Steidel C. C., Law D. R., Reddy N. A., 2010, *ApJ*, 719, 1168
 Fan X., 1999, *AJ*, 117, 2528
 Fukugita M., Ichikawa T., Gunn J. E., Doi M., Shimasaku K., Schneider D. P., 1996, *AJ*, 111, 1748
 Gibson R. R., Brandt W. N., Schneider D. P., 2008, *ApJ*, 685, 773
 Gilli R., Comastri A., Hasinger G., 2007, *A&A*, 463, 79
 Gilli R., Vignali C., Mignoli M., Iwasawa K., Comastri A., Zamorani G., 2010, *A&A*, 519, A92
 Glickman E. et al., 2012, *ApJ*, 757, 51
 Goad M., Koratkar A., 1998, *ApJ*, 495, 718
 Green R. F., Schmidt M., Liebert J., 1986, *ApJS*, 61, 305
 Greene J. E., Zakamska N. L., Smith P. S., 2012, *ApJ*, 746, 86
 Groves B. A., Dopita M. A., Sutherland R. S., 2004, *ApJS*, 153, 75
 Gunn J. E. et al., 1998, *AJ*, 116, 3040
 Gunn J. E. et al., 2006, *AJ*, 131, 2332
 Hainline K. N., Shapley A. E., Greene J. E., Steidel C. C., 2011, *ApJ*, 733, 31
 Hainline K. N., Shapley A. E., Greene J. E., Steidel C. C., Reddy N. A., Erb D. K., 2012, *ApJ*, 760, 74
 Hall P. B. et al., 2004, *AJ*, 127, 3146
 Hao L. et al., 2005, *AJ*, 129, 1783
 Hasinger G., 2008, *A&A*, 490, 905
 Hasinger G. et al., 2007, *ApJS*, 172, 29
 Hatziminaoglou E. et al., 2005, *AJ*, 129, 1198
 Heckman T. M., Ptak A., Hornschemeier A., Kauffmann G., 2005, *ApJ*, 634, 161
 Hewett P. C., Wild V., 2010, *MNRAS*, 405, 2302
 Hickox R. C., Markevitch M., 2006, *ApJ*, 645, 95
 Hines D. C., Schmidt G. D., Smith P. S., Cutri R. M., Low F. J., 1995, *ApJ*, 450, L1
 Hines D. C., Schmidt G. D., Gordon K. D., Smith P. S., Wills B. J., Allen R. G., Sitko M. L., 2001, *ApJ*, 563, 512
 Hopkins P. F., Hernquist L., Cox T. J., Di Matteo T., Robertson B., Springel V., 2006, *ApJS*, 163, 1
 Humphrey A., Villar-Martín M., Vernet J., Fosbury R., di Serego Alighieri S., Binette L., 2008, *MNRAS*, 383, 11
 Ivezić Ž. et al., 2002, *AJ*, 124, 2364
 Jia J., Ptak A., Heckman T., Zakamska N., 2012, preprint (arXiv:1205.0033)
 Jiang L., Fan X., Ivezić Ž., 2007, Richards G. T., Schneider D. P., Strauss M. A., Kelly B. C., *ApJ*, 656, 680
 Jiang L., Fan X., Vestergaard M., 2008, *ApJ*, 679, 962
 Khachikian E. Y., Weedman D. W., 1974, *ApJ*, 192, 581
 Khachikian É. Y., Weedman D. W., 1971, *Astrophysics*, 7, 231
 Kirkpatrick J. A., Schlegel D. J., Ross N. P., Myers A. D., Hennawi J. F., Sheldon E. S., Schneider D. P., Weaver B. A., 2011, *ApJ*, 743, 125
 Koekemoer A. M. et al., 2007, *ApJS*, 172, 196

- Korista K. T., Goad M. R., 2000, *ApJ*, 536, 284
 Kraemer S. B., Crenshaw D. M., 2000, *ApJ*, 532, 256
 Lawrence A., Elvis M., 2010, *ApJ*, 714, 561
 Lehmer B. D. et al., 2012, *ApJ*, 752, 46
 Liu X., Shen Y., Strauss M. A., Greene J. E., 2010, *ApJ*, 708, 427
 Liu G., Zakamska N. L., Greene J. E., Nesvadba N. P. H., Liu X., 2013, *MNRAS*, 430, 2327
 McCarthy P. J., 1993, *ARA&A*, 31, 639
 Marconi A., Risaliti G., Gilli R., Hunt L. K., Maiolino R., Salvati M., 2004, *MNRAS*, 351, 169
 Markwardt C. B., 2009, in Bohlender D. A., Durand D., Dowler P., eds, *ASP Conf. Ser. Vol. 411, Astronomical Data Analysis Software and Systems XVIII*, Astron. Soc. Pac., San Francisco, p. 251
 Mignoli M. et al., 2013, *A&A*, 556, A29
 Mushotzky R., 2004, in Barger A. J., ed., *Astrophysics and Space Science Library*, Vol. 308, *Supermassive Black Holes in the Distant Universe*. Kluwer, Dordrecht, p. 53
 Mushotzky R. F., Cowie L. L., Barger A. J., Arnaud K. A., 2000, *Nat*, 404, 459
 Nagao T., Maiolino R., Marconi A., 2006, *A&A*, 447, 863
 Nestor D., Hamann F., Rodriguez Hidalgo P., 2008, *MNRAS*, 386, 2055
 Norman C. et al., 2002, *ApJ*, 571, 218
 Oke J. B., Gunn J. E., 1983, *ApJ*, 266, 713
 Osterbrock D. E., Pogge R. W., 1985, *ApJ*, 297, 166
 Pâris I. et al., 2012, *A&A*, 548, A66
 Pier J. R., Munn J. A., Hindsley R. B., Hennessy G. S., Kent S. M., Lupton R. H., Ivezić Ž., 2003, *AJ*, 125, 1559
 Reyes R. et al., 2008, *AJ*, 136, 2373
 Richards G. T. et al., 2002, *AJ*, 123, 2945
 Richards G. T. et al., 2003, *AJ*, 126, 1131
 Richards G. T. et al., 2006a, *AJ*, 131, 2766
 Richards G. T. et al., 2006b, *ApJS*, 166, 470
 Richards G. T. et al., 2011, *AJ*, 141, 167
 Rieke G. H. et al., 2004, *ApJS*, 154, 1559
 Ross N. P. et al., 2012, *ApJS*, 199, 3
 Ross N. P. et al., 2013, *ApJ*, 773, 14
 Sandage A., 1965, *ApJ*, 141, 1560
 Sanders D. B., Soifer B. T., Elias J. H., Madore B. F., Matthews K., Neugebauer G., Scoville N. Z., 1988, *ApJ*, 325, 74
 Sanders D. B. et al., 2007, *ApJS*, 172, 86
 Schinnerer E. et al., 2004, *AJ*, 128, 1974
 Schlegel D. J., Finkbeiner D. P., Davis M., 1998, *ApJ*, 500, 525
 Schmidt G. D., Stockman H. S., Smith P. S., 1992, *ApJ*, 398, L57
 Schmidt M., Schneider D. P., Gunn J. E., 1995, *AJ*, 110, 68
 Schmidt G. D., Smith P. S., Hines D. C., Tremonti C. A., Low F. J., 2007, *ApJ*, 666, 784
 Schneider D. P. et al., 2010, *AJ*, 139, 2360
 Scoville N. et al., 2007, *ApJS*, 172, 1
 Shapley A. E., 2011, *ARA&A*, 49, 525
 Shapley A. E., Steidel C. C., Pettini M., Adelberger K. L., 2003, *ApJ*, 588, 65
 Smee S. A. et al., 2013, *AJ*, 146, 32
 Smith P. S., Schmidt G. D., Hines D. C., Cutri R. M., Nelson B. O., 2000, *ApJ*, 545, L19
 Smith P. S., Schmidt G. D., Hines D. C., Cutri R. M., Nelson B. O., 2002, *ApJ*, 569, 23
 Smith P. S., Schmidt G. D., Hines D. C., Foltz C. B., 2003, *ApJ*, 593, 676
 Soltan A., 1982, *MNRAS*, 200, 115
 Spergel D. N. et al., 2007, *ApJS*, 170, 377
 Steidel C. C. et al., 2002, *ApJ*, 576, 653
 Stern D. et al., 2002, *ApJ*, 568, 71
 Stern D. et al., 2005, *ApJ*, 631, 163
 Stern D. et al., 2012, *ApJ*, 753, 30
 Strauss M. A. et al., 2002, *AJ*, 124, 1810
 Sulentic J. W., Bachev R., Marziani P., Negrete C. A., Dultzin D., 2007, *ApJ*, 666, 757
 Takada M. et al., 2012, preprint (arXiv:1206.0737)
 Tran H. D., 1995, *ApJ*, 440, 565
 Treister E., Urry C. M., 2012, *Adv. Astron.*, 2012, 21
 Treister E. et al., 2009a, *ApJ*, 693, 1713
 Treister E., Urry C. M., Virani S., 2009b, *ApJ*, 696, 110
 Ueda Y., Akiyama M., Ohta K., Miyaji T., 2003, *ApJ*, 598, 886
 Urry C. M., Padovani P., 1995, *PASP*, 107, 803
 Vanden Berk D. E. et al., 2001, *AJ*, 122, 549
 Vasudevan R. V., Mushotzky R. F., Winter L. M., Fabian A. C., 2009, *MNRAS*, 399, 1553
 Vasudevan R. V., Fabian A. C., Gandhi P., Winter L. M., Mushotzky R. F., 2010, *MNRAS*, 402, 1081
 Vasudevan R. V., Brandt W. N., Mushotzky R. F., Winter L. M., Baumgartner W. H., Shimizu T. T., Schneider D. P., Nousek J., 2013, *ApJ*, 763, 111
 Vignali C., Alexander D. M., Gilli R., Pozzi F., 2010, *MNRAS*, 404, 48
 Villar-Martin M., Tadhunter C., Clark N., 1997, *A&A*, 323, 21
 Watson M. G. et al., 2009, *A&A*, 493, 339
 Williams R. J., Pogge R. W., Mathur S., 2002, *AJ*, 124, 3042
 Wright E. L. et al., 2010, *AJ*, 140, 1868
 Wu X.-B., Hao G., Jia Z., Zhang Y., Peng N., 2012, *AJ*, 144, 49
 Wuyts S., Cox T. J., Hayward C. C., Franx M., Hernquist L., Hopkins P. F., Jonsson P., van Dokkum P. G., 2010, *ApJ*, 722, 1666
 Xue Y. Q. et al., 2012, *ApJ*, 758, 129
 York D. G. et al., 2000, *AJ*, 120, 1579
 Yu Q., Tremaine S., 2002, *MNRAS*, 335, 965
 Zakamska N. L. et al., 2003, *AJ*, 126, 2125
 Zakamska N. L., Strauss M. A., Heckman T. M., Ivezić Ž., Krolik J. H., 2004, *AJ*, 128, 1002
 Zakamska N. L. et al., 2005, *AJ*, 129, 1212
 Zakamska N. L. et al., 2006, *AJ*, 132, 1496
 Zakamska N. L., Gómez L., Strauss M. A., Krolik J. H., 2008, *AJ*, 136, 1607

SUPPORTING INFORMATION

Additional Supporting Information may be found in the online version of this article:

Table 2. Table of 145 class A candidate type II quasars.

Table 3. Table of 307 class B candidate type II quasars.

Table 7. All *WISE* matches in our class A sample. Values are given in AB magnitudes.

Table 8. All *WISE* matches in our class B sample. Values are given in AB magnitudes (<http://mnras.oxfordjournals.org/lookup/suppl/doi:10.1093/mnras/stt1500/-/DC1>).

Please note: Oxford University Press are not responsible for the content or functionality of any supporting materials supplied by the authors. Any queries (other than missing material) should be directed to the corresponding author for the article.

This paper has been typeset from a $\text{\TeX}/\text{\LaTeX}$ file prepared by the author.